MSc Thesis in Mechanical Engineering

Flexible Alkaline Water Electrolysis

Flexibility limitations for transient electrolyzer operation

B.J. Lottman
2020

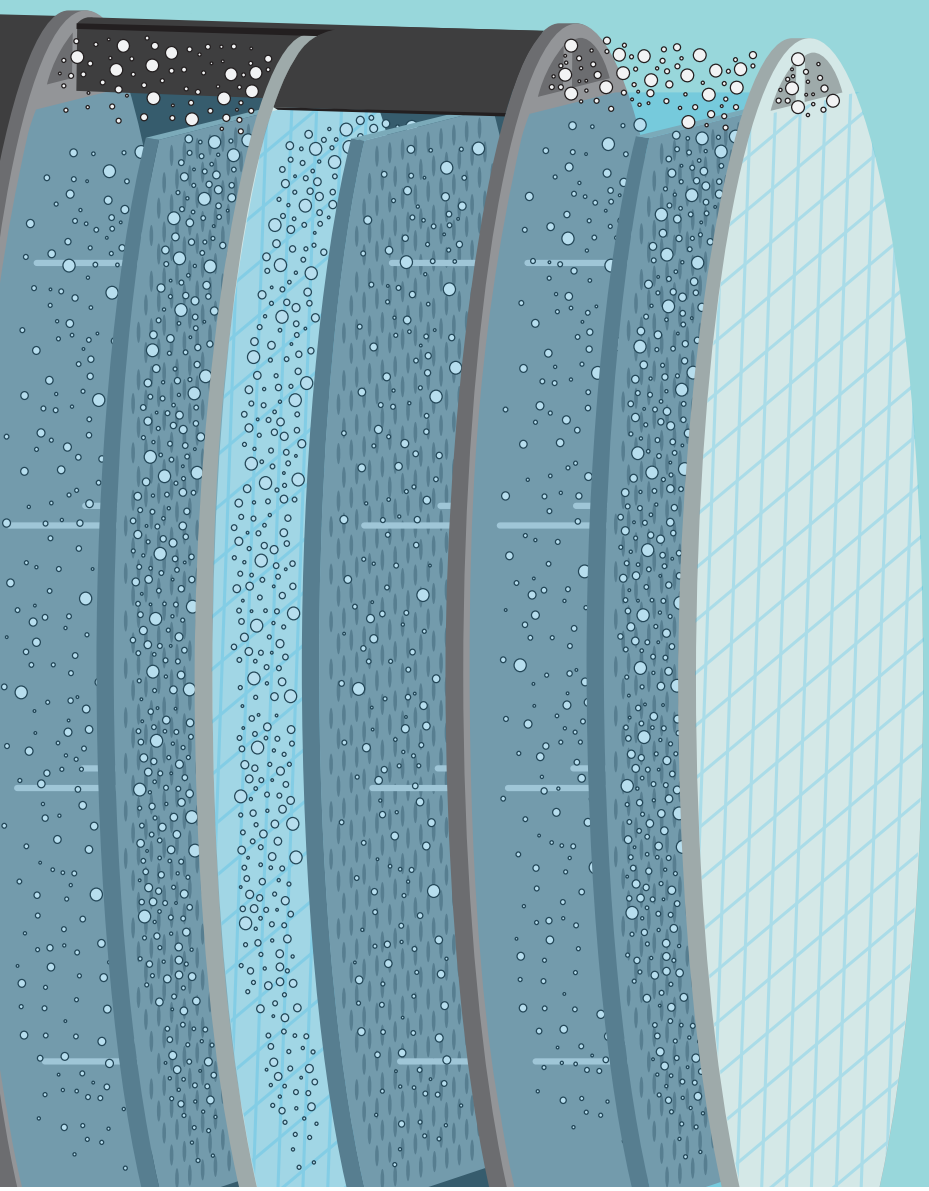

TU Delft
Nouryon

Flexible Alkaline Water Electrolysis

Flexibility limitations for transient electrolyzer operation

Public version due to third-party interests

MSc Thesis

to obtain the MSc title

at the Delft University of Technology,

to be presented publicly on Friday 13 November 2020

by

Bastiaan Joseph Lottman

Student Mechanical Engineering,
Delft University of Technology, Delft, The Netherlands.

This thesis has been supervised by

Supervisor TU Delft:	Ass. prof. dr. ir. J.W. Haverkort
Supervisor Nouryon:	Ass. prof. dr. ir. M.T. de Groot

Composition defense committee:

Chair:	
Prof. dr. ir S.A. Klein	Delft University of Technology & Nouryon
Members:	
Ass. prof. dr. ir. J.W. Haverkort	Delft University of Technology
Ass. prof. dr. ir. M.T. de Groot	Eindhoven University of Technology & Nouryon

An electronic version of this thesis is available at
http://repository.tudelft.nl/.

Contents

Abstract ix

Acknowledgements xi

1 Introduction 1

1.1 Context . . . 1
1.1.1 Hydrogen production . . . 1
1.1.2 Electrolyzers . . . 2
1.1.3 Flexible operation . . . 2
1.2 Nouryon . . . 3
1.3 Objective . . . 3
1.4 Scope . . . 3
1.5 Methodology . . . 3

2 Literature study 5

2.1 Basics . . . 5
2.2 Electrodes . . . 5
2.2.1 Configuration . . . 6
2.3 Electrolyte . . . 7
2.3.1 Gas holdup . . . 7
2.3.2 Conductivity . . . 8
2.4 Separator . . . 9
2.4.1 MacMullin number . . . 9
2.5 Complete system . . . 9
2.5.1 Separate flows . . . 9
2.5.2 Placement of the heat exchanger . . . 10
2.6 Electrolyzer modeling . . . 10
2.6.1 Electrochemical models . . . 10
2.6.2 Mass balance . . . 11
2.6.3 Heat balance . . . 11
2.7 Response rate . . . 12
2.7.1 Grid balancing . . . 12

3 NEL A485 plant 13

3.1 Stack . . . 14
3.2 Balance of Plant . . . 15
3.2.1 Gas-liquid separator . . . 15
3.2.2 Condenser . . . 15
3.2.3 Balancing Line . . . 15
3.2.4 Fresh feed . . . 15
3.2.5 Heat exchanger . . . 15

3.2.6 Controllers . . . 16
3.3 Available data . . . 16
4 Simulink model **17**
4.1 Model considerations . . . 17
4.1.1 Model type . . . 17
4.1.2 Timescale . . . 18
4.1.3 Modeling approach . . . 18
4.1.4 Physical properties . . . 19
4.1.5 Assumptions . . . 19
4.2 Stack . . . 20
4.2.1 Mass balance . . . 20
4.2.2 Electrochemical equations . . . 23
4.2.3 Thermal model . . . 28
4.3 Gas-liquid separator . . . 30
4.3.1 Mass balance . . . 31
4.3.2 Volumetric balance . . . 32
4.3.3 Thermal balance . . . 32
4.4 Pump . . . 33
4.4.1 Mass balance . . . 33
4.4.2 Thermal balance . . . 34
4.5 Heat exchanger . . . 34
5 Model validation **35**
5.1 Initial values and parameters . . . 35
5.2 Timestep . . . 35
5.3 Potential . . . 35
5.4 Temperature . . . 36
5.5 Liquid level . . . 36
5.6 Conclusion . . . 37
6 Steady state simulation **39**
6.1 Current variation . . . 39
6.1.1 Heat balance . . . 39
6.1.2 Potential . . . 40
6.1.3 Electrolyte concentration . . . 40
6.1.4 Efficiency . . . 41
6.2 Temperature variation . . . 42
6.2.1 Current potential curves . . . 42
6.2.2 Heat balance . . . 42
6.3 Maximum load overview . . . 42
7 Dynamic behavior simulation **45**
7.1 Situation 1: Ramp up from low load . . . 45
7.1.1 Thermal effects . . . 45
7.1.2 Mass effects . . . 46

7.2 Situation 2: Ramp down from full load . . . 47
7.2.1 Thermal effects . . . 47
7.2.2 Mass effects . . . 48
7.3 Situation 3: Ramp up from cold status . . . 50
7.3.1 Thermal effects . . . 50
7.3.2 Mass effects . . . 50
8 Discussion & Conclusions **53**
8.1 Flexibility limitations . . . 53
8.1.1 Liquid level . . . 53
8.1.2 Temperature . . . 55
8.2 Conclusions . . . 56
9 Recommendations **57**
9.1 Recommendations . . . 57
References **59**
A Appendix Net species transport example **63**
B Appendix Gas holdup rationale **64**
C Appendix Membrane properties **65**
D Appendix Convective heat dissipation **66**
E Appendix Reflection on simulation results **67**
F Appendix Step time analysis **70**
G Appendix Demiwater feed flow **71**
H Appendix Heat balance at different temperatures **72**
I Appendix NEL Ramp claim assessment **73**
J Appendix Preliminary comparison: Gas holdup **74**
K Appendix Preliminary calculation: Backflow **75**

Nomenclature

Acronyms

AE	Alkaline Electrolysis	
AEME	Anion Exchange Membrane Electrolysis	
BoP	Balance of Plant	
PEME	Proton Exchange Membrane Electrolysis	
SOE	Solid Oxide Electrolysis	

Greek Symbols

α	charge transfer coefficient	-
ζ	yearly efficiency loss	%
ϵ_g	emissivity	-
η_f	Faraday efficiency	-
η_{act}	overpotential	V
ε_g	gas holdup	-
κ	conductivity	W/m^{2}K
ν	stochiometric coefficient of species i for $z = 2$	-
σ_B	Stefan-Bolzmann constant	5.67×10^{-8} W/m^{2}K^4

Roman Symbols

A	surface area	m^2
a	age of stack	years
A	pre-exponential component Arrhenius eq.	-
b	Tafel slope	V
$\bar{c}_p$	molar heat capacity	J/molK
c	concentration	mol/m^3
c_p	densimetric heat capacity	J/kgK
d	distance	m
E	activation energy	J/mol
F	Faraday's constant	96485 C/mol
$\bar{G}_f$	molar Gibbs free energy	J/mol
$\bar{h}$	specific molar enthalpy	J/mol
$\bar{H}_f$	molar enthalpy of formation	J/mol
I	current	A
j	current density	A/m^2
j_0	exchange current density	A/m^2
L	height	m
LL	liquid level	%
M	molarity	mol/L
m	mass	kg
$\dot{n}$	molar flow rate	mol/s
N_{cells}	Number of cells per stack	-
n_i	amount of mols of component i	mol
N_M	MacMullin number	-
p	pressure	kPa
$\dot{Q}$	heat flow	J/s

Q	heat	J
R	universal gas constant	8.314 J/mol K
r	radius	m
$R_{subscript}$	resistance	Ω
s	entropy	J/mol K
T	temperature	K
$\bar{V}$	molar volume	m^3/mol
$\dot{V}$	volumetric flow rate	m^3/s
V	potential	V
V	volume	m^3
z	amount of electrons transferred in reaction to form 1 mol H_2	2 -

Subscripts

act	activation
amb	ambient
a	anodic side
BL	balancing line
$cell$	single cell composed of 2 compartments
$comp$	compartment
$conv$	convective
c	cathodic side
deg	degraded
df	demiwater feed
eff	effective
eld	electrode
eq	equilibrium
$evap$	evaporation
ext	exterior
far	faradaic
gh	gas holdup
GLa	anodic gas-liquid separator
GLc	cathodic gas-liquid separator
G	gaseous fraction
H_2O	water
H_2	hydrogen
HEX	heat exchanger
in	inflow
i	species i
lye	electrolyte
L	liquid fraction
max	maximum
mix	mixed flow from the pump
O_2	oxygen
ohm	ohmic
out	outflow
pot	potential
rad	radiative
R	reaction
sep	separator diaphragm
$stack$	stack, all cells electrically connected
tn	thermoneutral
tot	total

Abstract

A numerical model is developed in Simulink to simulate transient alkaline electrolyzer operation. The model is built to simulate a large scale hydrogen plant in Rjukan, Norway. The model is based on physical relations where available, some plant-specific data is modeled using empirical equations. The model describes the anodic and cathodic compartments using electrochemical equations, lumped heat, and a perfectly mixed mass model. The balance of plant is modeled using the same heat and mass model. The model can predict the potential, temperature, efficiency, temperature, and mass flows and is validated using 30 days of measured data of the large scale plant. Transient current input, such as sudden current ramp up from 0 to 100% load, is used to simulate dynamic operation. From these simulations flexibility limitations of the electrolyzer are determined. The results suggest that the liquid levels in the stack and gas-liquid separator and temperature are limiting flexibility. The liquid levels form the biggest limitation of dynamic operation due to potential flooding or draining of the gas-liquid separators.

Acknowledgements

I would like to thank my supervisors Willem Haverkort and Thijs de Groot for their support, help, guidance, and especially patience during my often unstructured disquisitions. The help with structuring both my thoughts and writing was invaluable for finalizing this thesis. I would like to thank Nouryon for offering me the opportunity to work in an innovative environment. The insights gained from speaking with employees of a company having so much practical experience in hydrogen production have been very valuable in the creation of this thesis. I would like to thank my family for all the love and support that I have received to the point of finalizing my studies. I would like to highlight my parents that have unconditionally supported me both emotionally, with a 'kick in the butt' when needed, and financially during my studies. I would like to thank Renske for being my love and care during the last years of my study. Finally, I would like to thank all my friends, especially my roommates, who have been very patient and supportive while the coronavirus made us stay at home.

B.J. Lottman
Delft, October 2020

1

Introduction

1.1. Context

The energy transition, which strives to change the energy supply from fossil to non-carbon based sources, brings many challenges. One of the challenges is the seeming impossibility to supply a baseload if the energy supply is solely provided using green production. The variable nature of the resources, e.g. solar and wind, makes it unreliable as baseload. Since a baseload is seen as an important feature in the distribution of electricity it will be necessary to create ways to ensure this is possible.

Temporary storage of electricity could provide a baseload. It would allow system operators to maintain grid balance and ensure stable supply in periods with low generation. The expectation is that long-term (seasonal) energy storage can be achieved by using carbon-based fuels, hydrogen carrying fuels or hydrogen. Light chemicals such as carbon-free produced ammonia (Afif et al., 2016), hydro-power or batteries may be used instead of carrier molecules.

It is likely that hydrogen plays an important role as energy carrier in our future (IEA, 2019). If not for large scale storage or transportation means, applications will be developed for processes that are impossible to electrify. Many industrial processes require (hydrocarbon) fuels to form the process product. In many industrial processes, fuel does not only provide energy, but also the feedstock for product formation. Currently, most fuels stem from a fossil source, but in the future, these can be formed using green hydrogen.

1.1.1. Hydrogen production

Most hydrogen (ca. 95%) is produced industrially using methane reforming (Rostrup-Nielsen and Rostrup-Nielsen, 2002). Methane and steam are fed into a reactor at very high temperatures (700 to 1100 °C). Here, the endothermic water-gas shift reaction occurs:

$$CH_4 + H_2O \Leftrightarrow CO + 3\ H_2 \qquad \Delta H^{o}_{298} = 206 \text{kJ/mol} \tag{1.1}$$

The carbon monoxide oxidises in a slightly exothermic reaction to form even more hydrogen.

$$CO + H_2O \Leftrightarrow CO_2 + H_2 \qquad \Delta H^{o}_{298} = -41 \text{kJ/mol} \tag{1.2}$$

In such a process, other fractions such as ethanol, propane and even gasoline could be used for catalytic reforming to produce hydrogen.

For production of hydrogen, many technologies are being considered that do not co-produce CO_2 as a waste stream. The most promising technologies are currently thermochemical cycles, BM gasification and electrolysis (Guban et al., 2019). Electrolysis of water is a much anticipated solution to replace fossil based hydrogen production. This is a process where an electric direct current (DC) drives an otherwise non-spontaneous chemical reaction, splitting water into oxygen and hydrogen using an electrolyzer.

1.1.2. Electrolyzers

An electrolyzer is a fairly simple device that performs electrolysis. Many different types exist, but they all share the following basic components. Two electrodes are in contact with a conductive liquid or solid soaked in a conductive liquid. This conductive liquid is a solution that allows certain ionic species to be transported through the fluid. Often a solid wetted diaphragm is placed in the middle, separating the two products of the reaction and allowing certain dissolved components to pass. At the electrodes half reactions take place. On the anode an oxidation reaction will occur at the surface creating a free electron. The free electron will travel to the cathode via an external circuit where a reduction reaction will occur. During the oxidation reaction at the anode an ion is formed. This charged ion will travel through the electrolyte and diaphragm to react at the opposite surface. Depending on the cell type different ions will be transported to the opposite electrode.

Only two of several types of electrolysis can be considered as mature technologies: Proton Exchange Membrane Electrolysis (PEME) and Alkaline Electrolysis (AE). Others, such as Solid Oxide Electrolysis (SOE) and Anion Exchange Membrane Electrolysis (AEME), are in earlier stages of development and need significant progress before commercial adoption will be feasible (Junginger and Louwen, 2020).

Alkaline & Proton Exchange Membrane Electrolyzers

In 1888 an industrial method was developed for water electrolysis by engineer Dmitry Lachinov. By 1902, more than 400 industrial water electrolyzers were in operation. These electrolyzers used alkaline solutions. By applying a potential, water is split in hydrogen and oxygen via two half reactions. During this process, OH^- ions are generated at the cathode and travel through the cell to the anode. The conductive liquid is aqueous potassium hydroxide (KOH) or aqueous sodium hydroxide (NaOH) in concentrations of 20-35 wt%.

In previous years technology using solid polymer membranes has been the subject of research more and more. In this kind of electrolysis an acidic electrolyte is present. In this cell, H^+ ions are transported over a wetted solid polymer membrane. An advantage often named is the fast ramp up and down time. Due to the use of many different rare metals controversy exists around the large scale application of this technology in regard of price and available supply.

1.1.3. Flexible operation

The electricity consumption of an electrolyzer depends on its operating load and temperature. The electricity costs to produce electrolytic hydrogen contribute to more than 92% of the total costs. Industrial practice is to reduce electricity consumption by sourcing cheap heat from industrial plants nearby that generate heat as a waste by-product (Douglas et al., 2012). Higher temperatures allow for more efficient operation and therefore lowers electricity costs. A cold electrolyzer cannot quickly ramp up due to several phenomena.

- At low temperatures the increased resistance leads to higher potentials and therefore considerable efficiency losses.
- Peak voltage arising during fast ramp up or a pressure rise due to the sudden generation of hydrogen can harm the cell.

To improve the flexibility and prevent damage to the cells proper dynamic thermal models should be developed. Efficiency optimization is highly important due to the high energy consumption of electrolyzers.

Currently, the flexibility in alkaline electrolyzers is about 10%/min (Schmid, 2018), while full ramp up and down within a minute would be ideal. Accurate models have to be developed to ensure the creation of reliable business cases to exploit the variability of energy supply. Most models are developed for steady state operation. These are generally not able to predict the dynamic behavior of electrolyzers as time variant phenomena prevail. An important phenomenon is the thermal behavior of the stack.

1.2. Nouryon

The thesis presented here was carried out for the TU Delft at Nouryon. Nouryon has made a large effort to provide as much data as input for this research. Nouryon (formerly AkzoNobel Specialty Chemicals) is a company delivering essential chemicals worldwide. Nouryon is currently cooperating with partners to realize the future of hydrogen. On of their projects, the ALKALIFLEX project, is focused on increasing the flexibility and production capacity of alkaline water electrolysis. As a follow up on the ALKALIFLEX project, this thesis aims to further develop a technical understanding of the challenges in flexible operation. Nouryon has many years of experience in chlor-alkali electrolysis and has been running a medium-large scale (8MW) water electrolysis plant in Norway since 1992.

1.3. Objective

It proves challenging to operate conventional AE as dynamically as PEME, but the capital expenditure of AE in which simple materials are used is much lower than for PEME cells. There has not been any need to develop dynamically operated AE systems in the past due to a constant power supply. This has changed due to an irregular supply by solar- and wind-generated power. Models are needed to simulate the behavior of these systems and research should strive to push this technology to the next level. The objective of this research is the development of a dynamic model of alkaline water electrolysis. The limiting factors can be addressed by modeling parameters during transient operation. An estimation of the dynamic behavior can then be made. This model should contain the electrochemical, thermal and mass effects of fast ramp-up and ramp-down. These considerations lead to the main research question:

How are operational parameters of alkaline hydrogen production, such as potential and temperature, influenced by transient operation?

A model will be created to simulate dynamic behavior to answer the main research question. Several sub-questions leading to the answer on the main question are to be answered:

- *What factors are limiting fast ramp times?*
- *Should ramp rates be limited?*
- *How will ramp rates influence operational parameters, thermal behavior in particular?*
- *Should the stack be allowed to cool down during low-load operation or be actively heated?*

1.4. Scope

This thesis focuses on atmospheric alkaline water electrolysis. This technology is the most commercially proven method due to its age and simplicity. From the beginning of this research, some data was available from an operational plant in Rjukan, Norway. This plant consists of 4 electrolyzers similar to the NEL A485 design. The parameters of the electrolyzers are described in detail in Chapter 3. Although not all information about these cells is known, many parameters have been estimated from measurements, operational data and earlier research. This data will be used as input for the dynamic model. This research will focus on describing an AWE plant with a 25% KOH solution. The electrolyzer will be fed with a transient input. As many physical relations as possible will be used to describe the dynamic behavior of such a plant.

1.5. Methodology

Operational data of the electrolyzer has been provided by Nouryon. This data consists of the potential, current and temperature as a function of time. First, an electrochemical model of the stack was built. In order to validate this stack model, the measured temperature and current are used as input. The synthetically generated potential is then compared to the actual potential.

Once the potential shows good agreement the rest of the stack is modeled. This is the addition of the mass and thermal balances to the model. The model will then be run using the measured current as input. To validate the thermal and mass balances the simulated temperature will be compared to the measured temperature.

The stack model is then incorporated in a larger system where the other equipment is modeled to form the complete electrolyzer. The model allows to simulate the dynamic behavior. Only recently detailed data such as the liquid level of the anodic gas-liquid separator has been acquired and will be compared to the model to estimate the effect of plant control.

The model will then be used to run steady state and transient simulations. The limiting factors of transient operation will be defined from the simulations.

2

Literature study

2.1. Basics

In Alkaline Water Electrolysis two electrodes are placed in an aqueous electrolyte solution, also called lye. The electrodes are often made from stainless steel treated with a nickel-containing catalyst (Millet and Grigoriev, 2013) to improve activation at the surface. At each of these surfaces a half reaction occurs depending on the type of cell. A semi-permeable diaphragm is placed at the center of the cell in most electrolyzers. An image of a typical alkaline electrolysis cell can be found in Figure 2.1.

The electrolyte allows ions to travel from the electrode on one side of the cell to the opposite electrode. In the case of AE, the lye in the cell is an alkaline solution of potassium hydroxide (KOH) or sodium hydroxide (NaOH) in water. This solution allows for OH- ions to be transported through the cell. Free electrons are generated at the anode and transported via an external circuit to be "consumed" at the cathode.

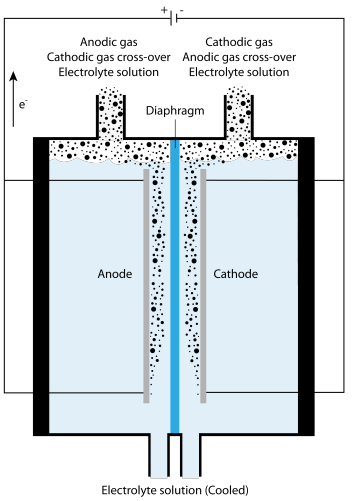

Figure 2.1: Simplified model of a bipolar electrolysis cell

The following reactions occur:

Cathode:

$$4H_2O + 4e^- \rightarrow 2H_2 + 4OH^- \tag{2.1}$$

Anode:

$$4OH^- \rightarrow O_2 + 2H_2O + 4e^- \tag{2.2}$$

Overall equation:

$$2H_2O \rightarrow 2H_2 + O_2 \qquad \Delta\bar{G}_f = 237 \text{ kJ/mol } H_2 \tag{2.3}$$

2.2. Electrodes

Steel grids are usually used as a basis for the electrodes. These grids are often treated with a coating to improve reaction kinetics. The coatings in AE are often made of a nickel-based catalyst. An example is Raney Nickel, a very porous Ni-Zn material where the zinc is leached from the alloy (Millet and Grigoriev, 2013).

2.2.1. Configuration

For alkaline electrolysis two configuration types have been developed: Monopolar and bipolar plate configurations. A monopolar (also called unipolar) cell consists of electrodes hanging in a bath of lye. The anodes and cathodes are connected in parallel electrically. This way the electrolyzer can be operated at high current and low potential. In a bipolar configuration, the cells are connected in series. Therefore the plate in between two cells forms the anode for the first cell and the cathode for the adjacent cell. This allows for operation at low current and high potential (Tilak et al., 1981). Typical images of both types can be found in Figure 2.2.

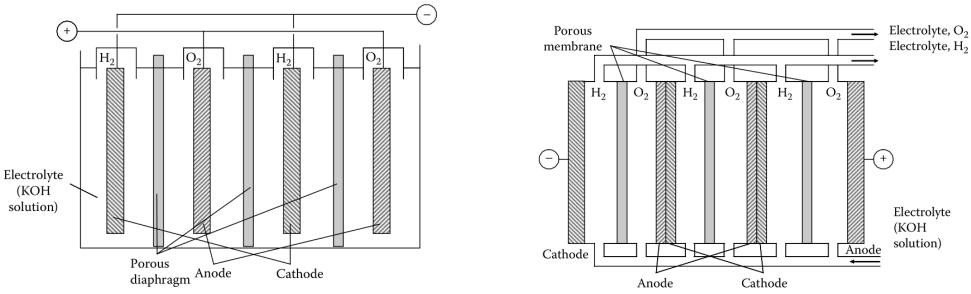

(a) Unipolar configuration

(b) Bipolar configuration

Figure 2.2: Electrolyzer configuration examples, ref. from Kasahara (2011)

Although bipolar plate configurations are dominant, both types are still used around the world. Each of the configurations has its own (dis)advantages. Some of the advantages of unipolar and bipolar electrolyzers are the following (Oluf Jensen, 2008).

For unipolar electrolyzers:

1. They are relatively simple and cheap to build, which comes at the price of lowered efficiency compared to more advanced electrolyzers. Therefore they are often viable options when electricity prices are low.
2. When a cell needs maintenance, the rest of the stack can continue to operate as the cell can simply be bypassed. This saves costs and optimizes downtime.

For bipolar electrolyzers:

1. They can be operated at high potential operation due to the cells being connected in series. Operation at high current decreases ohmic losses (Santos et al., 2013).
2. They are better suited for high temperature and pressure operation due to the bipolar plates offering increased structural strength.

Probably the biggest reason why bipolar electrolyzers are used more often is the fact that the stack can be operated at higher voltages, requiring less transformation. The electrodes are bolted on the bipolar plate with a gap in between of roughly 10-30 mm. The electrodes are perforated to let some bubbles and lye flow through the electrode to prevent local overheating and big temperature differences from the bottom to the top half of the electrolyzer cell. The electrode itself is located at a short distance of 1-3 mm from the diaphragm.

When the path length of currents in an electrolyzer becomes smaller, the accompanying resistance decreases. A type of cell where the path length is reduced to a minimum is called a zero-gap electrolyzer. In these cells, the electrode is placed directly against the separator, in theory completely eliminating the electrolyte resistance outside the separator.

2.3. Electrolyte

The electrolyte is conducting the ions through the cell. Depending on the concentration of KOH or NaOH molecules dissolved in the liquid, the conductivity changes. Typically in alkaline electrolysis a concentration of 25 wt% to 30 wt% is used. During operation, water is consumed by the reaction. At the same time the product gasses also extract water vapor from the system due to its vapor pressure. The ions will not evaporate and remain dissolved in the liquid. A very small amount of KOH leaves the system. The velocity of the product gas stream can cause drops of lye to be dragged along. In order to maintain sufficient liquid in the system, freshwater is added to the system.

2.3.1. Gas holdup

When the electrolyzer is operated, hydrogen and oxygen gas are being produced. In steady state simple equations can be used to describe the in- and outgoing flows as no mass buildup is possible over time. However, if an electrolyzer is operated dynamically, the amount of mass inside the system can change. An important phenomenon during transient operation is the gas holdup. Figure 2.3 shows an example of liquid level rise in a soda bottle due to formation of gas (red dotted line). If these bubbles are continuously formed, eventually the system would settle (see image D and E) and a certain fraction of the volume would consist of gas bubbles in the liquid. This is called the gas holdup.

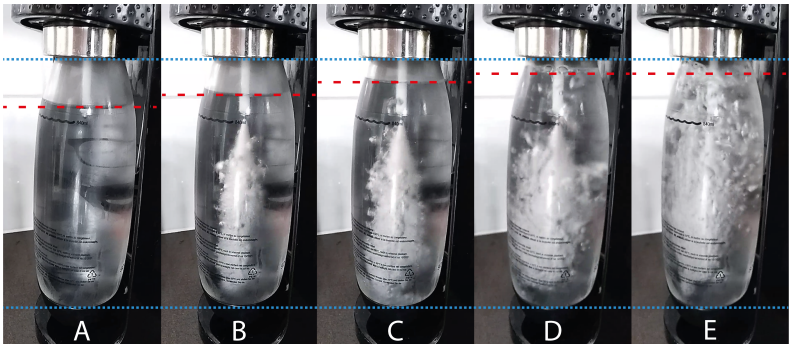

Figure 2.3: Increase of the liquid level due to increase in gas holdup

The gas holdup causes the volume of the lye in the stack to increase when gas is produced. The gas holdup is determined by many factors such as stack temperature, current density, surface structure of the catalyst, gap size and subsequent bubble size. As described by Kellermann et al. (1998), the coalescence barrier effect prevents the formation of bigger size bubbles, which in turn has an effect on the rise velocity of the bubbles. Funk and Thorpe (1969) states that the gas holdup is dependent on the slip ratio, which is often unknown. Caspersen and Kirkegaard (2012) have shown similar results using a model describing electrolyte with only natural convection. They have shown the electrolyte conductivity to exponentially decrease from the bottom to the top approaching a limiting value. This is caused by the increased path length due to produced gas, which is influenced by the current, pressure and subsequent rise velocity.

Because of the uncertainty of the amount of gas holdup, some research describes experiments to determine the bubble fraction as listed below. This can be done using several methods such as optically analyzing the bubble formation on electrodes, analyzing the bubble behavior at the outlet of the cell and measuring the increase in resistivity of the electrolyte during operation. Although these methods give an estimation of the gas holdup, all are subject to assumptions and specific conditions. Almost all experiments and CFD analyses are performed on small cells up to 40 cm height such as in Zarghami et al. (2020). Kreysa and Kuhn (1985) have experimentally shown the gas holdup to level off and it seems that for each gas-electrolyte combination a limiting gas holdup exists. Therefore the local gas holdup will increase from the bottom up, but at a certain height, the limiting gas holdup will be reached and will be constant over the remaining height of the cell. The mentioned article by Kellermann et al. (1998) shows that this limiting gas holdup increases with electrolyte concentration, potentially explaining measurements of very high gas holdup of 0.6-0.7 in some experiments. With sufficient liquid flow the maximum can be kept well below the limiting values. The influence of the height of a cell is therefore likely not that important and could be the reason for the lack of experiments on a larger scale. Research is being performed by Seibel and Kuhlmann (2018) using cells with the same height as used in commercial plants.

2.3.2. Conductivity

The conductivity of the electrolyte is a measure of the ease of transfer of ions through the fluid. The conductivity is given as a function of the weight concentration and temperature. The conductivity of aqueous KOH is measured by various researchers. The measurements by Hine (1985) are given in Figure 2.4. The temperature usually starts to vary during dynamic operation. An increasing temperature results in a higher conductivity.

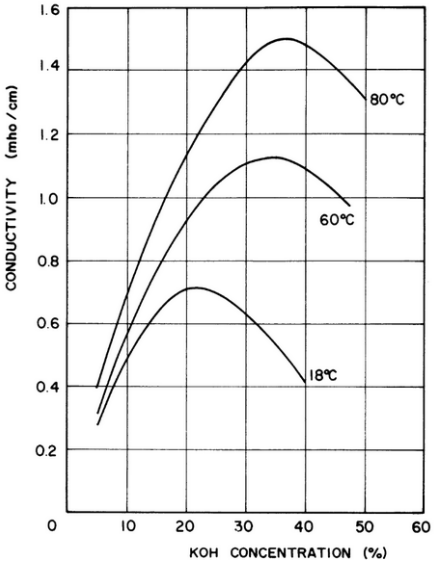

Figure 2.4: Electrolyte conductivity of KOH solutions, copy from Hine (1985)

The conductivity of the electrolyte is influenced by the presence of bubbles. The gas bubbles have a very low conductivity and therefore increase the length of the pathway that electrons have to travel through the electrolyte, represented in Figure 2.5. Therefore the resistance of a fluid with a higher gas holdup will be higher. It could be seen as the lye becoming a porous medium (see Electrolyte conductivity in section 4.2.2) and from that theory, the resulting increased resistance could be determined. One of the main conditions is that the properties of the voids of the considered medium are known. Although a lot of research is conducted, due to strong dependence on the materials and fluids used, the effect of the bubble diameter is still disputed (Sequeira et al., 2013). From optical bubble analysis by Haug et al. (2017) the bubble size seems to become constant above certain current densities. A correction factor for the increased path length can be described using the Bruggeman equation and is only valid for non-homogeneous sized spherical voids (Tjaden et al., 2016).

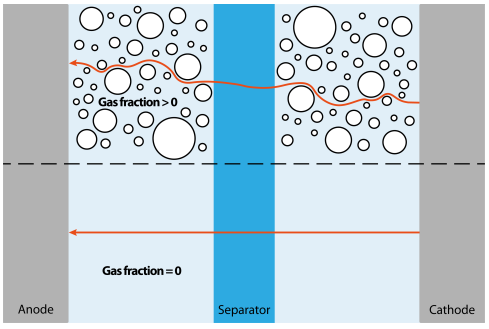

Figure 2.5: Influence of bubbles on the path length and therefore resistance

2.4. Separator

A separator diaphragm separates the cathode and anode side. It prevents hazardous mixtures of generated gases to be formed, but creates an increased resistance for electrons. Conventionally asbestos diaphragms were used, but after discovering their carcinogenic effects, a Zirfon PERL diaphragm has been developed consisting of a polysulfone matrix and the addition of ZrO_2 (Vermeiren et al., 1998).

This diaphragm is wetted easily, which means that the material has a tendency to be in contact with water. This is important, not only because water molecules should be transported through the diaphragm, but moreover, hydroxide ions can only be conducted if the diaphragm is wetted. Although the diaphragm is a good ionic conductor, resistances arise in the diaphragm. In addition to the conductivity of the electrolyte used, the separator conductivity varies based on the material and manufacturing method. This depends on several properties, such as but not limited to the porosity, permeability and tortuosity of the separator. These properties are all affecting how well a certain structured material is able to let liquids or gasses flow through. Since many properties like void pore-size often follows a distribution range it is hard to calculate these properties physically. Therefore porous separator properties are usually experimentally determined. Schalenbach et al. (2016) have determined cross-permeation limits of a Zirfon PERL separator.

2.4.1. MacMullin number

Another way to describe the quality of porous media such as the ionically conducting diaphragm is by determining the MacMullin number. MacMullin and Muccini (1956) have defined this dimensionless value relating the conductivity of the electrolyte to the conductivity of the porous diaphragm soaked in electrolyte. In Separator conductivity in section 4.2.2 this will be further elaborated upon.

2.5. Complete system

Most of the previous information is about the stack itself. In reality, an electrolyzer is the whole plant consisting of the stack connected to other equipment. The rest of the equipment is often called the Balance of Plant (BoP). Multiple configurations for AE exist, but the equipment used is almost always the same:

- Gas-liquid separator
- Heat exchanger
- Pump (optional, in some cases natural convection is used to circulate lye)
- Scrubber/dryer (optional, depending on further use of hydrogen)
- Compressor (optional, depending on further use of hydrogen)

Two main configurations are commonly seen. A configuration where the lye streams are kept separate and one where these are recombined after the product gases have been removed.

2.5.1. Separate flows

The system where the lye streams are kept separate has the benefit that the amount of invasive gas remains a lot lower than would be the case without separate flows, as can be seen in Figure 2.6. This is due to the fact that the lye will contain dissolved hydrogen and oxygen when leaving the gas-liquid separators. Because the flows are then mixed, they will cause an indirect cross over. It has been shown by Trinke et al. (2018) that the hydrogen crossover is particularly influenced by the mixing of lye from the cathodic and anodic compartment.

On the other hand, because water is consumed on the cathodic side and produced on the anodic side, the electrolytes are concentrated and diluted respectively. Since both compartments should remain equally leveled demiwater has to be added on the cathode side and lye should be able to flow from the anodic to the cathodic side.

2.5.2. Placement of the heat exchanger

The heat exchanger can be placed at several positions in the system. If the heat exchangers were placed before the gas-liquid separation, they would have to process a large flow due to the gas present. Not only would the heat transfer be less efficient, also two separate exchangers would be needed. On the other hand, gas-liquid separation would occur at a lower temperature, potentially eliminating the need for a cooling step after separation.

The heat exchanger can also be placed after the gas-liquid separators. If separate flows are used, two heat exchangers would be needed, whereas, for a mixed flow, only one is required. Depending on the desired operation range and further processing of the hydrogen, one of these configurations is chosen.

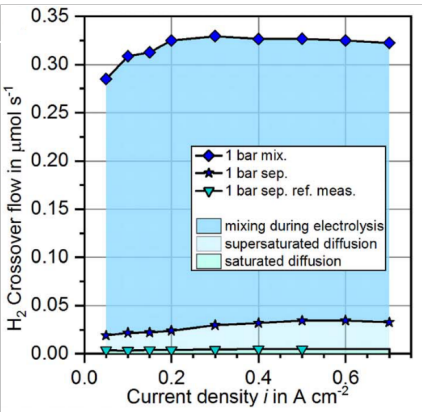

Figure 2.6: H_2 crossover for mixed and separated electrolyte cycles, ref. from Trinke et al. (2018).

2.6. Electrolyzer modeling

Electrolyzer modeling has been performed on many different scales. From research on the effect of surface structure on the reaction kinetics to complete systems including the electricity generation and hydrogen demand. In this research, the stack including BoP will be considered. Since the stack is the 'heart' of the process it is necessary to build a reliable electrochemical model and apply this in a bigger system including heat exchangers, separators and other equipment. Therefore literature has been considered describing detailed physical models to be combined into one big model describing overall atmospheric behavior.

2.6.1. Electrochemical models

A review by Olivier et al. (2017) states that static approaches are prevalent when looking at electrochemical models. The electric response time of an electrolysis cell is relatively fast compared to that of the complete system. The response can be described by either empirical or physical models.

One of the most widely known models is a semi-empirical AE model by Ulleberg (2003) that has been used a lot as a base in further research. This model determines the polarization curve with parameters that have been experimentally fitted using only temperature as operational variable. Although the model can determine the polarization curve accurately, the model is a mathematical treatment of experiments and therefore bears no physical meaning. Many parameters affecting electrolysis are not taken into account and experiments need to be performed to create such a model. Since this research developed a framework to be filled in with more meaningful physical equations, further research includes several modifications. Amores and Carreras (2014) for example have extended the model to include electrolyte concentration and distance between the electrodes in the ohmic resistance term and shows only a 0.8% error term using experiments. In the same manner Sánchez et al. (2018) and Olivier et al. (2017) have reviewed models describing many more modifications, such as cell architecture, pressure, electrolyte concentration or flow rate. By adding more and more corrections to the model, the model will slowly start to look like a model describing all effects in a physical manner but based on empirical relations.

A lot of research has been done on physical equations describing electrochemical behavior. Building a model this way requires a lot of information regarding equipment, materials, methods and conditions used. To illustrate this, consider the fact that a few measurements could form the basis of a simple empirical model. On the other hand, when describing every part physically, a large error could already occur if a different electrode material or size would be considered. Many different physical approaches exist and where some authors assume parts to be negligible, others do not. Many authors have reviewed or developed physical models (Abdin et al., 2017; Brauns and Turek, 2020; Götz et al., 2016; Le Bideau et al., 2019; Olivier et al., 2017; Henao et al., 2014; Wang et al., 2014; Zeng and Zhang, 2010). Many of them share the same basis but differ in how detailed some phenomena are modeled and at what level experimental data is used. For example, the increased resistivity caused by gas holdup in the electrolyte can be determined empirically but also by calculating the estimated increased path length as mentioned above. In chapter 4 the equations used in the model of this thesis have been specified.

2.6.2. Mass balance

For mass balance models are found describing phenomena on very different levels. Because so many phenomena are involved in multi-phase systems, detailed models have been developed describing only parts of the cell. An example is the model by Haug et al. (2017), which describes the mass transfer to and from the boundary layer and between two phases in the cell. Using a fitted relation the gas evolution at the reaction surface is determined from the current density. The produced gas will either transfer to the bulk of the electrolyte in dissolved form or generate bubbles at the electrode interfaces. Subsequently, the impurities due to crossover and gas holdup in the bulk electrolyte are determined. Experimental analysis has shown that steady state situations are accurately described by this model as can be seen in Figure 2.7c. From experiments the fits shown in Figure 2.7a and 2.7b were determined for the gas holdup.

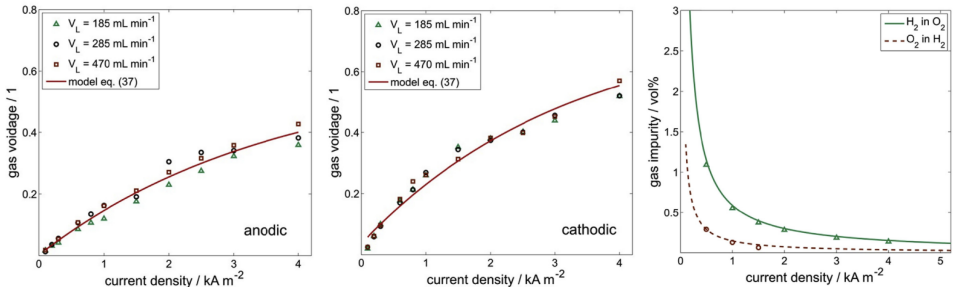

(a) Anodic gas holdup for different flow rates at c_{KOH} = 28.6wt%

(b) Cathodic gas holdup for different flow rates at c_{KOH} = 28.6wt%

(c) Gas impurities for different current densities at c_{KOH} = 31.7 wt% and $\dot{V}_L$ = 330 mL/min

Figure 2.7: Comparison of experimental and simulated results at $T = 80$ °C, ref. from Haug et al. (2017)

Abdin et al. (2017) have developed a model at a higher level which is more commonly found in literature. They describe a one-dimensional alkaline model which describes perfectly mixed compartments separated by porous separators (including the electrodes). It describes the electrochemical equations and mass balance on a physical basis where possible. The model is built in Simulink and forms a basis which could be implemented pretty easily in larger models. The simulations show good agreement with the HRI and PHOEBUS experimental data.

Only very recently, David et al. (2020) has developed a highly detailed phenomenological dynamic model describing all mass flows individually, including volume mass, energy and friction balances. The system describes a self pressurized system with separated lye flows. The response in the gas-liquid separators to a valve opening or current change can be simulated. Comparing measured data and the model, the author states that the model yields an adequate representation of the behavior but by improving the controller a better fit during fast changes could be obtained.

2.6.3. Heat balance

If the mass and electrochemical balance are known, determination of the thermal behavior is straightforward. The electrochemical equations lead to a potential over the stack. If the potential representing the energy consumed by the reaction including the reaction heat, is subtracted from the cell potential the excess potential can be found. If this potential is then multiplied with the current, the excess energy transformed to heat can be determined. The temperature and composition of the cell are known from the mass balance. Using the heat generation, the subsequent thermal balance can be determined.

Two types of thermal models are commonly used: models using discretized parts of the cell and models using the lumped thermal capacity. The latter is most prevalent and straightforward. Hug et al. (1993) have used a previous version of VDI-GVC (2010) to calculate the thermal response. Most lumped models are determined only on stack scale. Some models are comprised of the complete system including all the auxiliary equipment, but this requires much more information about the system.

Heat losses are often influencing behavior. Textbooks on heat transfer offer many correlations depending on shapes, fluids and materials considered. The heat loss can be determined by calculating heat transfer coefficients based on the case-specific correlations. From the surface temperature and materials the radiative heat transfer can also be determined.

2.7. Response rate

As mentioned before, probably due to the invariability of energy supply in current applications of electrolysis, flexibility of AE never needed to improve. With an increasing renewable energy supply penetration, the flexibility of its balancing agents should also increase. The question is: How much? The grid an electrolyzer system is connected to very much determines the requirements of the system.

Lüke and Zschocke (2020) mention alkaline systems to be typically very robust and as long as the rest of the system is designed for the swift change in flows, a ramp up of 50% of the maximum energy capacity can be achieved in less than a minute. Full load can be achieved within minutes.

2.7.1. Grid balancing

If an electrolyzer would be directly coupled to a wind farm, the flexibility requirement will be less than when connected to a solar PV system. Milan et al. (2013) has listed maximum ramps for certain timespans, to be found in table 2.1. This is data generated from 8 months of measured data of a 12 wind turbine farm at an undisclosed location.

Most extreme increment	τ = 1 s	τ = 8 s	τ = 32 s	τ = 128 s
Wind speed u_τ (m/s)	3.5	11.1	11.4	14.7
Turbine power P_τ (%)	24.8	82.5	106.6	108.8
Farm power $P_{farm,\tau}$ (%)	8	22.8	33	55.3

Table 2.1: Absolute value of the most extreme increments measured over a time scale τ during the measurement period of 8 months. The power increments are given in percent of the corresponding rated power for the turbine and the farm. Occasional overshoots slightly above rated power justify power increments larger than 100% (Milan et al., 2013).

These values are quite extreme when compared to research by Huber et al. (2014). They have shown that the net load ramp for a country-wide grid with a hypothetical supply of 100% wind energy is at max 25%/h of the maximum load. When solar PV is taken into account these ramp rates will increase.

For power system operations, down-ramps are generally more challenging to manage than up-ramps. This is because upward wind (or solar) power ramps can be managed more easily such as tuning down other generators' schedules, increase demand or even curtailment if necessary. However, when downward power supply ramps occur, power system operators have to compensate for the deficit of wind (or solar) power by increasing other generating capacities which is often harder.

If an electrolyzer system would be used for grid balancing activities to benefit from low electricity prices during times of high supply, the relevance of fast in- or decrease of load depends on the timescale considered. If the European energy market is assumed to be balanced using a day-ahead, 1-hour and 5-min market (Ortner and Totschnig, 2019), response times of systems can be given an order of magnitude. It would be logical to assume that a switch to 100% of the load will be required during a grid balancing event. If the ramp time from completely cooled down is over an hour, it does not make sense to operate on a market shorter than that time unless the lower energy prices outweigh the decreased efficiency of the cell. Although energy consumption or the deliberate lack thereof is one of the goals of grid balancing operation, the produced hydrogen is what eventually makes operation profitable. A business case should therefore determine the optimal moment for ramp up or down.

3

NEL A485 plant

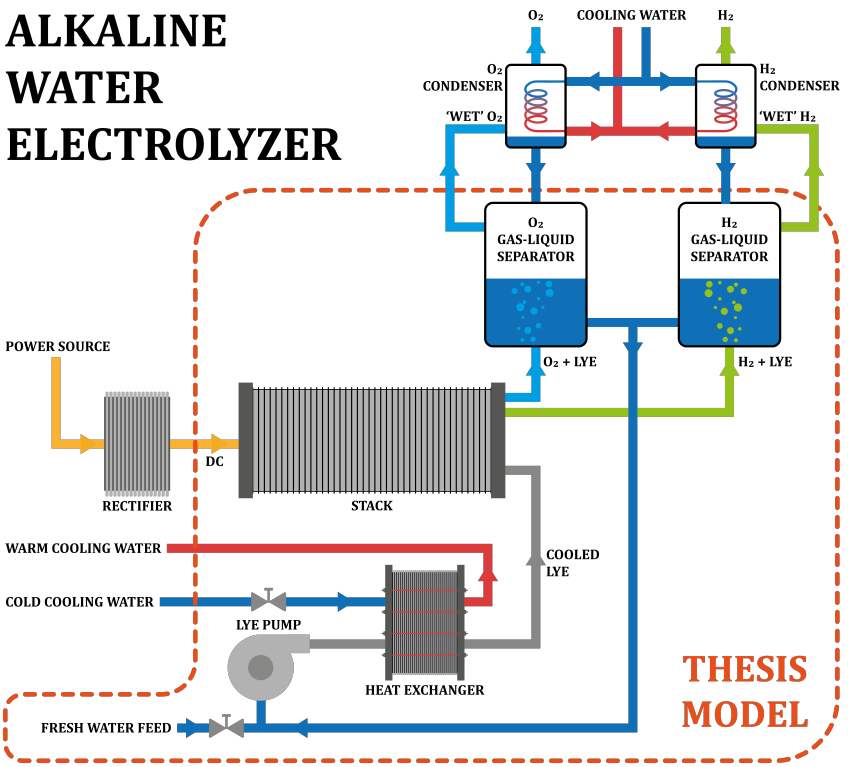

Figure 3.1: Illustrated schematic overview of the system in Norway and the subsystem considered in this thesis

The dynamic model describing the behavior of the electrolyzer plant requires many equations as well as constants, properties and input parameters. Many parameters are imposed by the design of the plant, these are described in this chapter.

Within the realm of AE many types of electrolyzers exist and for each one dynamic behavior will be different. Therefore the curves, constants and other parameters need to be adjusted for the specific electrolyzer. The case considered in this thesis is a NEL A485 electrolyzer.

This system consists of rectifiers that supply the power to the stack of a fixed number of electrically connected cells in series. The product streams are fed to gas-liquid separators, the gaseous fraction will go to the condensers and the liquid will be pumped through a heat exchanger and back to the stack. In Figure 3.1 an overview of the system can be found. The part considered to be modeled in this thesis is

shown in the orange dotted box.

3.1. Stack

As mentioned before, the stack is the 'heart' of the system and will be described first. The stack configuration is a filter press bipolar cylindrical cell. A picture of the exterior and a simplified cut out overview can be found in Figure 3.2.

Each cell is separated by stainless steel bipolar plates. A current is applied to the bipolar plate at the very end of the stack, which results in a potential drop over each cell due to its connection in series. The system has electrodes, indicated by the orange line in Figure 3.3, bolted to both sides of the bipolar plate. The electrodes on either side form the cathode and anode of the two adjacent cells. These electrodes are submerged in the electrolyte and hang at a few millimeters from the separator. From the measurements given in Figure 3.3, the area of the electrode can be determined. The electrodes are perforated in reality, the details of these holes are often unknown and the effects on the behavior are not clear. It should be noted that it is common to express the current density as a function of the electrode area without accounting for the holes. This convention has also been used in this thesis.

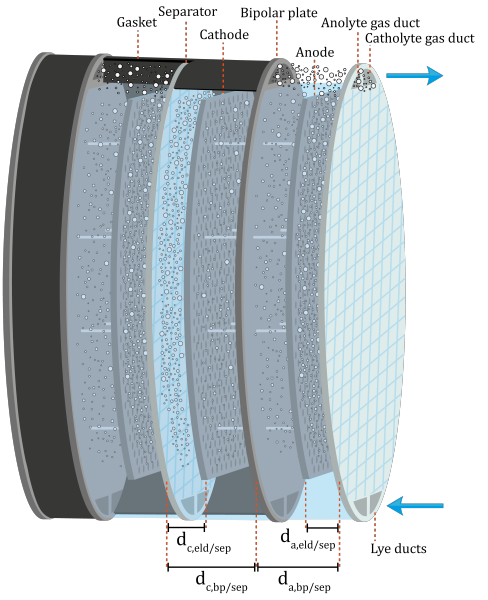

Figure 3.2: Illustrated schematic overview. The thickness, width and radius are not to scale

Cooled electrolyte is fed via channels, called lye ducts, through the stack. The gasket contains very small channels connecting the lye ducts to the anodic and cathodic compartment at the bottom of the cell. These channels have to remain very small to reduce shunt current, current 'leaking' away through this channel. This shunt current will be elaborated upon in section 4.2.2.

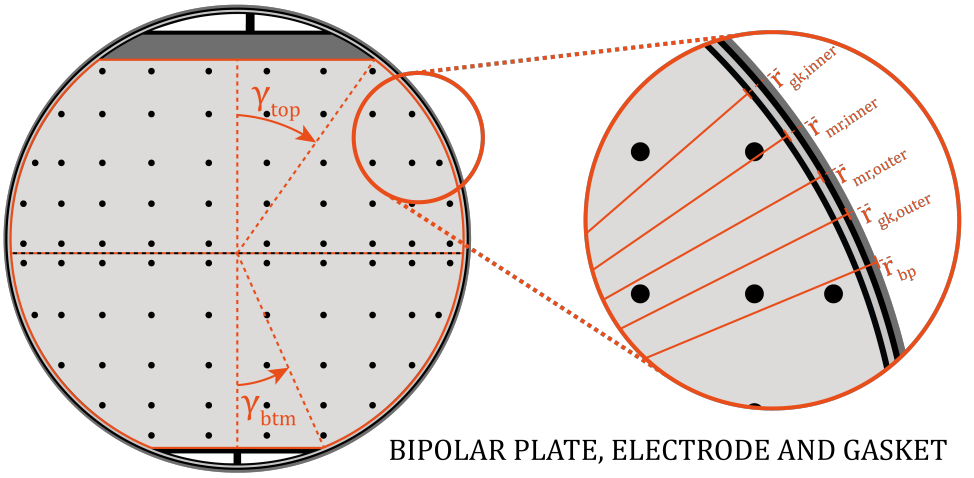

Figure 3.3: Dimensions of the stack electrodes and gaskets

The produced gas and excess lye is leaving the compartment via the gas ducts. The feed stream temperature is controlled in order to keep the stack operating at set temperatures. A factor to keep in mind here

is the fact that a temperature difference of roughly 35 °C is allowed between the in- and outgoing flows. This is to prevent a large temperature gradient over the height of the cell. This could lead to unequal thermal expansion of the cell walls, potentially causing leakage. At a fixed circulation rate, the maximum temperature difference will limit the maximum heat generation during operation.

3.2. Balance of Plant

The balance of plant consists of all equipment in Figure 3.1 besides the stack. In this thesis, only the gas-liquid separators, heat exchanger and pump will be taken into account since these will form the bulk of the energy and mass flows. It should be kept in mind that in reality, the condensers affect the thermal behavior and mass flows but will be neglected here due to their small contribution.

3.2.1. Gas-liquid separator

The gas-liquid separators are vessels of 5.8 m^3 where the product stream from the stack and condensate stream from the cooling of the product flow into. The product stream from the stack is entering the gas-liquid separator below the liquid level and the gas subsequently bubbles upwards to the surface. The liquid level is measured and is used as the controlling parameter for the fresh feed. Since no mixing of the product gases should occur, separate tanks are used for hydrogen and oxygen. No active cooling or heating happens in these tanks, so the temperature is determined by the incoming flows and heat dissipation to the exterior.

3.2.2. Condenser

The gaseous fraction includes a certain amount of water vapor and is therefore fed through a condenser. Here the product gas is cooled down and the bulk of the water vapor condenses and flows back to the gas-liquid separator. Due to the relatively small mass flow and heat capacity of gases, the condenser has been excluded from the model.

3.2.3. Balancing Line

The liquid parts of the two gas-liquid separators are connected via a balancing line. On one side of the diaphragm water is produced whereas on the other side water is consumed. This way one separator would be emptied and the other filled over time. The balancing line makes sure the two liquid levels are such that the pressure is equal at the bottom of the liquid column, where the gas ducts feed the product stream to the separators. This is important because by doing so, the pressure in the cells remains equal on both sides to prevent hazardous crossover or even rupture of the diaphragm.

3.2.4. Fresh feed

From the gas-liquid separators the streams are mixed with a demiwater stream to replenish the water consumed by the overall reaction. The liquid feed is activated when the liquid level in the anodic gas-liquid compartment drops below a certain threshold. Freshwater is then fed to the system until a second threshold is reached. The liquid feed is estimated to be 3.6 m^3/h from the liquid level measurements, which will be elaborated upon in section 5.5.

3.2.5. Heat exchanger

The liquid from the separators and the demiwater feed are mixed and pumped through a plate heat exchanger. The pump supplies a constant circulation and is not controlled in any way. The temperature of the lye is controlled by varying the amount of cooling water flowing through the plate heat exchanger. After cooling, the lye is fed to the stack via the lye ducts. No data is available for either the temperature of the flows through the heat exchanger or the cooling water flow. From discussions with experts, a practical limit is implied where the maximum temperature difference between the in- and outgoing flow is 35 °C. This is to prevent leakage due to differences in thermal expansion over the height of the stack and possibly other effects such as decreased efficiency in the cooler part of the stack.

3.2.6. Controllers

Two valves in the system are controlled by measured parameters. The first valve is the freshwater feed, this valve is controlled by the liquid level sensor in the anodic gas-liquid separator. From the detailed measurements described in section 3.3 it is found that the fresh feed valve is opened whenever the liquid level in the anodic gas-liquid separator drops below 32% and closes when the system reaches a level above 34%.

In regard to the cooling water control, based on the outflow temperature of the stack the cooling is set to a certain level. The exact controller settings are unknown, but based on the detailed measurements and comparison, the settings of a PI-controller have been estimated. Using these settings the comparison has been performed between the simulation and reality.

3.3. Available data

The data was made available by Nouryon. This data comes from one of the 4 stacks of the plant in Rjukan, which has number 3003 and is shown in Figure 3.4. The data has been recorded roughly every 1.5 hours for 30 days. This dataset will be called dataset 1. Other data points such as the purity of the two gas streams and the liquid level of the gas-liquid separator were also provided. Although the interval is far out of the timeframe considered in this research, the timeframe was short enough to see the temperature in- and decrease with time and the other parameters could be seen to vary. Using dataset 1 the model comparison was performed initially.

Figure 3.4: Stack 3003 at the production location in Rjukan, Norway

During the research new data was acquired. For day 3 to 13 of the 30 days of the dataset acquired earlier, data points for an interval of 60 seconds were obtained. This set is called dataset 2. Since the model should describe the behavior of the system in the scale of minutes or even seconds this data yields a lot of insight in the response of the system. This data is much more detailed.

The available data in dataset 1 and dataset 2 consists of the following:

- Current supplied to the stack
- Temperature of the cathodic stream out of the stack
- Potential over the stack
- Pressure at the top of the anodic gas-liquid separator
- Pressure at the top of the cathodic gas-liquid separator
- Liquid level in the anodic gas-liquid separator

4

Simulink model

4.1. Model considerations

Many models describe the behavior of the electrolyzer using empirical relations. Although some pretty accurate models have been developed using these relations, these bear no physical meaning and do therefore not add to the fundamental understanding of phenomena playing a role in these systems. Although not possible everywhere, an effort will be made to express as many properties using physical relations.

4.1.1. Model type

A choice to be made is the kind of model that is to be developed. This is related to the objective of the research. Depending on the conditions and the program used, it becomes easier to model the system. Usually, easier-to-use software comes at the cost of lower freedom. The following considerations have been taken into account when deciding on the program to be used.

The model will describe the behavior of the system which is calculated by using properties of several fluids at different temperatures and pressures. Therefore it is necessary to incorporate fluid properties and although this can be done by hand, more convenient methods would be welcome. The model has to be dynamical and accordingly, the program should be able to handle differential equations. Since a numerical model will be built, the program should be able to give a clear overview of the model and preferably automatically graph relevant property curves. Several programs/languages allow for this kind of modeling such as Python, Matlab/Simulink, Aspen Plus/HYSYS and TRNSYS. From these, two were compared in greater detail: Aspen and Matlab.

Aspen software is often used in the process industry to model complete systems. The advantage of using this software is that it allows building a model with a very clear overview of the plant. The databases for many fluids and mixtures are incorporated with the software making its use very convenient. The downside is that although a clear overview of the model and its components is available, the equations solved for each subsystem, such as a gas-liquid separator, are harder to see as these are already incorporated in the software. The solver optimizes runtime by determining the order of equations to be solved. The way the solver handles the system equations can cause the system to become unsolvable, making working with the model especially hard for people who have not built the model themselves. Also for non-standard operations, custom blocks need to be programmed in Aspen Custom Modeler.

Matlab Simulink also offers a way to create a clear overview of the process. It is more labor-intensive to model the fluid properties and blocks because the system of equations has to be determined completely by the researcher. On the other hand, it is easier to follow the modeling steps, also within the blocks. The system of equations is solved in a more straightforward way and the developer can build the model to be as robust as desired. The stack itself should be hard coded for both software options. Therefore Simulink was chosen as the software for this research.

4.1.2. Timescale

As I have previously stressed, the timescale on which the response is required determines the level of modeling. The double-layer effect for example describes the time lag of the voltage when the current suddenly changes due to accumulating charge in the electrode-electrolyte interface (Ursúa and Sanchis, 2012). The fast response of this double layer effect is only relevant in sub-second response times and settles within a second. It does not make sense to incorporate this if it is desired to create a model to describe the response within seconds to minutes.

The phenomena to be modeled using differential equations are parameters that cannot be assumed to reach steady state within seconds. Since the scope of this thesis is about grid stabilizing operation, the model to be built will be to simulate behavior in the order of magnitude of seconds to minutes. This means that dynamic operation behavior should be analyzed when the following events occur:

- Ambient temperature startup to full load
- Operation at minimal load (turn-down ratio)
- Ramp up and down during regular operation

The effects of the events above are simulated in chapter 7.

4.1.3. Modeling approach

The model consists of several sub-models that are combined to describe the behavior of the electrolyzer. The components are shown in Figure 4.1. The stack and gas-liquid separators are modeled as continuously stirred tank reactors.

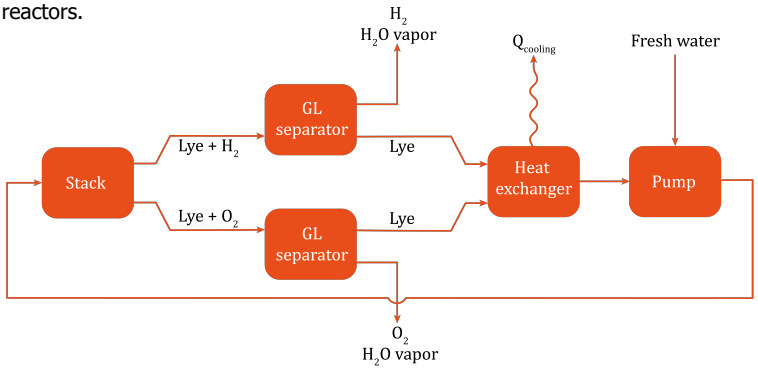

Figure 4.1: An overview of the blocks and flows to be modeled in Simulink

In each of the blocks, the mass and thermal balance will be solved. An electrochemical model will be used to calculate the reaction products in the stack. The pump and heat exchanger are modeled by simply combining the outflows of the separators and the freshwater feed. In Figure 4.2 an overview of the parts of the stack can be seen.

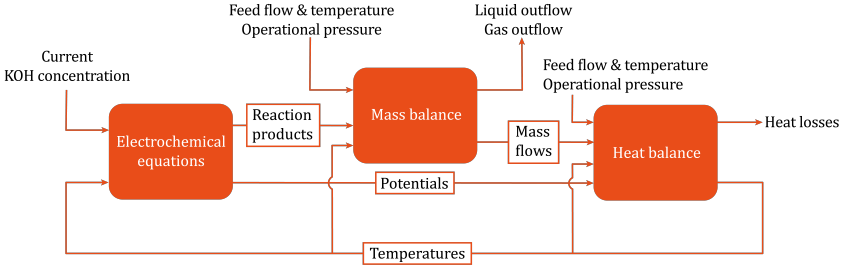

Figure 4.2: An overview of the stack model with connecting flows

4.1.4. Physical properties

In order to model the system, the properties of the fluids present in the system need to be determined. To retrieve the thermophysical properties regarding fluids and mixtures the 'REFPROP.m'-file[1] will be used to read values from NIST REFPROP. Since KOH mixtures are not present in this library, other sources have been used to determine the properties (Davis et al., 1967; Gilliam et al., 2007; Haynes et al., 2014; Hine, 1985; Schalenbach et al., 2018).

4.1.5. Assumptions

In the following sections, the model equations are written for each sub-part of the model. For some of these to be valid certain assumptions have to be done. These are listed here.

- Gases are ideal: Since the cell is operated at low pressures around 1 atm and temperatures below 100 °C, the ideal gas law is assumed to be applicable.
- The compartments are assumed to be perfectly mixed: Each cell consists of two compartments. According to experiments by Boissonneau and Byrne (2000) the multi-phase flow is assumed to be turbulent due to bubble formation. Therefore the compartments are assumed to be perfectly mixed.
- Perfect separation of the gas and liquid occurs in the gas-gas-liquid separators: The gas-liquid separators will separate the produced gases from the liquid. The residence time is assumed to be sufficient to cause perfect separation.
- Equal pressure and in the anodic and cathodic compartments: The balancing line at the bottom of the gas-liquid separators will equalize the pressure. The outlets from the top of the stack are also connected at the bottom of the separators. The pressure in the compartments is assumed to be equal.
- The stack has a uniform temperature: The separator and bipolar plates are very thin and a good heat conductor respectively. In addition the surface areas within the cell are large. Therefore, heat transfer between the compartments will be efficient. The two compartments, bipolar plates and separator are assumed to have equal temperatures allowing a lumped-element model to be used for the heat balance.
- The crossover through the separator is zero: Because the pressure is equal on both sides no convective crossover will be present. Diffusive crossover in turn is neglected so no crossover is assumed through the diaphragm. The crossover of OH^- is not zero because this is required for the reaction.
- The heat capacity of gases is neglected: Because the density of gases is small compared to liquids, the influence of these on the mass and thermal balance is very small. The heat capacity of gas has therefore been neglected.
- The liquid in the gas-liquid separator is not able to flow back into the stack compartments.

[1] Open source mapping, created by P. Brown (Ramgen Power Systems, Inc.), J. Lux (German Aerospace Center), C. Muzny (NIST), E. Lemmon (NIST) and K. Wait (GE Appliances)

4.2. Stack

In this section the model of the stack will be described. The stack consists of 230 cells. The model will describe one cell and has to be multiplied by the amount of cells to get results for the complete stack. The mass, current and thermal balance are described in each subsection.

4.2.1. Mass balance

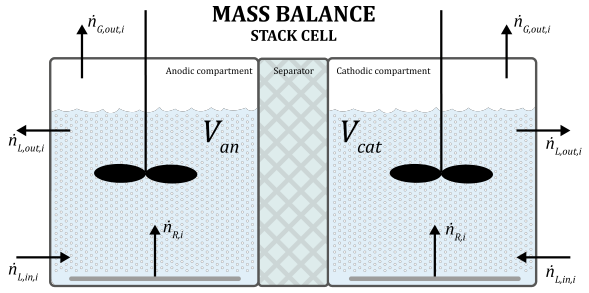

Figure 4.3: Mass balance overview of the electrochemical cell

The cell is separated by a Zirfon PERL separator, thus creating two compartments: an anodic and cathodic compartment. The electrolyte in each of these compartments is called the anolyte and catholyte respectively. At the electrodes of the compartments hydrogen, oxygen, dissolved hydroxide ions and water are produced or consumed. These species are either dissolved in the bulk electrolyte or form gas bubbles and rise to the gas-liquid surface in the compartment. The separator is porous for the electrolyte and its dissolved species. A pump actively circulates electrolyte. The circulating lye flow is bigger than the consumption of water in the stack. The outgoings flow will not only contain the product gases and water vapor but also electrolyte. From the stack this flow will enter the gas-liquid separator.

The material balance is defined by summing all in- and outgoing flows and the generation or consumption for each compartment. The total molar in- or decrease of species i in a compartment in timestep dt is given by the following material balance.

$$\frac{d}{dt}(n_i) = \dot{n}_{net,i} + \dot{n}_{R,i} \tag{4.1}$$

Here n_i is the total amount of moles i present in one timestep, $\dot{n}_{net,i}$ is the net molar flow rate of species i given in eq. 4.2 and $\dot{n}_{R,i}$ is the molar reaction consumption or production rate of i given in eq. 4.7.

Net species transport

The net flow of a species i only takes into account fractions present in flows that enter (in) or leave the cell (out). Since crossover is not taken into account, only the lye feed from the pump and the multiphase flow to the gas-liquid separator add to the net molar mass balance of species i. The net molar flow of species i can be expressed by summing the fractions in the liquid (L) and gaseous (G) fractions.

$$\dot{n}_{net,i} = \dot{n}_{L,in,i} - \dot{n}_{L,out,i} - \dot{n}_{G,out,i} \tag{4.2}$$

where $\dot{n}_{L,in,i}$ and $\dot{n}_{L,out,i}$ are the liquid or dissolved molar in- and outflow of species i and $\dot{n}_{G,out,i}$ is the molar gaseous outflow of species i. The incoming stream of a compartment is always single phase and therefore no incoming gaseous fraction is present in eq. 4.2.

The molar in- and outflow of the liquid or dissolved species i for each compartment can be calculated with the following formula's.

$$\dot{n}_{L,in,i} = \dot{V}_{L,in} c_{in,i} \tag{4.3}$$

$$\dot{n}_{L,out,i} = \dot{V}_{L,out} c_i \tag{4.4}$$

where $\dot{V}_{L,in}$ and $\dot{V}_{L,out}$ are the volumetric in- and outflow (see eq. 4.17 and 4.18) and $c_{in,i}$ and c_i the molar concentration of the inflow and compartment respectively.

The produced gases and water vapor are present in the bubbles generated. The gaseous fraction will be at saturated water vapor pressure for the compartment temperature and electrolyte concentration. The

rest is filled with product gas. Using the partial pressure the gaseous molar outflow of species i $\dot{n}_{G,out,i}$ can be described as follows.

$$\dot{n}_{G,out,i} = \frac{\dot{V}_{G,out}}{RT_{cell}} p_i \tag{4.5}$$

Here p_i is the partial pressure of species i, T_{cell} the temperature of the cell and R the universal gas constant. The volumetric outflow $\dot{V}_{G,out}$ can be determined by eq. 4.15.

The partial pressure p_i of the gaseous part in the stack can be determined from the pressure imposed by the rest of the design, which we will call p_{stack}. It is assumed that only water vapor and the product gas of that compartment are present in the gaseous fraction. Using p_{stack} and by determining the temperature dependent partial pressure of water vapor above the lye p_{H_2O}, the partial pressure p_i of the produced gas can be determined. The graph used to determine the partial pressure can be found in Appendix A

$$p_{stack} = p_i + p_{H_2O} \tag{4.6}$$

Reaction rate

The amount of oxygen and hydrogen produced and water consumed can be determined using Faraday's law (eq. 4.7).

$$\dot{n}_{R,i} = \eta_f \frac{\nu_i j A_{eld}}{zF} \tag{4.7}$$

Where $\dot{n}_{R,i}$ is the amount of mol of species i consumed or produced in the reaction (R), η_f the Faradaic efficiency, ν_i the stochiometric ratio of species i consumed or produced per mol hydrogen formed, j the current density, A_{eld} the electrode area, z the amount of electrons consumed to form one hydrogen molecule and F the Faraday constant.

The stochiometric ratio ν_i for $z = 2$ is given below.

Anodic compartment	$\nu_{O_2} = 0.5$	$\nu_{H_2O} = 1$
Cathodic compartment	$\nu_{H_2} = 1$	$\nu_{H_2O} = -2$

Gaseous and liquid fractions

Before continuing it is important to understand how the gaseous and liquid volumes are related in the compartments of the cell. During operation a gas holdup is present in the electrolyte. V_{lye+gh} is the volume of the electrolyte including the gas holdup. The amount of gas $V_{G,gh}$ and liquid V_{lye} in V_{lye+gh} can be determined using eq. 4.9 and 4.10. From the compartment volume V_{comp} and liquid volume V_L, the total gaseous volume in the cell V_G can be determined. This gaseous volume consists of the volume of the gas holdup $V_{G,gh}$, determined using gas holdup ε_g, and the void above the liquid level $V_{G,g}$ if present. A schematic overview is shown in Figure 4.4.

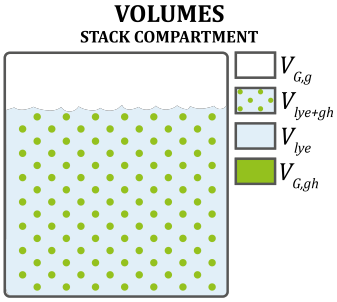

Figure 4.4: A schematic overview of the volumes present in a compartment

$$V_{G,g} = V_{comp} - V_{lye+gh} \tag{4.8}$$

$$V_{G,gh} = \varepsilon_g V_{lye+gh} \tag{4.9}$$

$$V_L = V_{lye} = (1 - \varepsilon_g) V_{lye+gh} \tag{4.10}$$

$$V_G = V_{G,gh} + V_{G,g} \tag{4.11}$$

$$V_{comp} = V_L + V_G \tag{4.12}$$

Gas holdup

Relations for the gas holdup by Haug et al. (2017) are used as average gas holdup for the space before and behind the electrode in the Simulink model. In Appendix B the reasoning is elaborated upon. The general equation is given in eq. 4.13.

$$\varepsilon_{g,max} = X_1 - X_2 \cdot X_3^{(j/1000)} \tag{4.13}$$

Here $\varepsilon_{g,max}$ gives the maximum gas holdup. Two fits are used for the anodic and cathodic compartment. The parameters of the fits can be found in Table 4.1. According to the author the fits represent the gas holdup accurately at current densities larger than 300 A/m^2.

Compartment	X_1	X_2	X_3
Anode	0.59438	0.59231	0.75647
Cathode	0.76764	0.73233	0.73457

Table 4.1: Parameters used to estimate the gas holdup in the compartments (Haug et al., 2017)

In order to model the system when the current density changes, the rate of increase in gas holdup will be limited by the volumetric production rate of the gas during ramp up. Before the ramp up the liquid level is at the top op the cell. If a ramp up occurs the maximum gas holdup increases. At that moment however, the actual gas holdup in the cell lower than the empirical value indicates. The actual gas holdup can only increase if gas is produced to replace the liquid volume. Since it takes time for the cell to produce enough gas to increase the gas holdup to the new steady state amount, the following limitation has been used. The gas holdup will be limited by the amount of gas present in the cell V_G if this is smaller than the maximum gas holdup would suggest.

$$\varepsilon_g = \min\left(\frac{V_{G,gh}}{V_{comp}}, \varepsilon_{g,max}\right) \tag{4.14}$$

During ramp down the gas holdup decreases and the liquid level drops, which happens within seconds due to the weight of the lye. The liquid fraction will start to increase but is limited by the volumetric inflow of liquid, evaporation and consumption (only at the cathode). The liquid level will slowly increase until V_{comp} is equal to V_{lye+gf}. If that happens the liquid level has reached the top of the cell and the lye starts to flow out.

In many electrolyzers the liquid from the gas-liquid separators cannot flow back into the stack due to the use of a riser. It is unknown if a riser is present in the system in Rjukan. In this case it has been assumed that no backflow is possible from the gas-liquid separators.

Volumetric balance

The total amount of moles of each species n_i in one timestep can be determined by integrating eq. 4.1. This will be done for the liquid and gaseous fraction separately. The amount of gas present cannot exceed the volumetric capacity of the cell so the excess gaseous volume will flow out of the cell. The gaseous outflow is determined using the following equation.

$$\dot{V}_{G,out} = \frac{d}{dt}\left(V_G - \frac{RT_{cell}}{p_{stack}} \sum n_{G,i}\right) \tag{4.15}$$

Here the rightmost term represents the total volume of all gaseous species at the end of the timestep. The liquid volumetric outflow of electrolyte can be determined using the following equation.

$$\dot{V}_{L,out} = \frac{d}{dt}\left(V_{lye} - \sum n_{L,i}\bar{V}_i\right) \tag{4.16}$$

Here $\bar{V}_i$ represents the molar volume of species i. The rightmost term represents the total volume of all liquid including dissolved species at the end of the timestep. No gas is assumed to be present in the feed

stream. The volumetric feed is therefore imposed by the circulation pump which provides the volumetric flow for 2 compartments.

$$\dot{V}_{in} = \frac{1}{2}\dot{V}_{pump} \tag{4.17}$$

All that is left to do now is, enter the initial values of the liquid levels and feed a transient current density. Using these all volumetric flows are known the whole system of equations can be solved including the total outgoing volumetric flow rate $\dot{V}_{out}$. The values calculated are used as input for the next timestep.

$$\dot{V}_{out} = \dot{V}_{L,out} + \dot{V}_{G,out} \tag{4.18}$$

4.2.2. Electrochemical equations

As can be seen from eq. 4.7 the current density j is the key parameter in hydrogen generation. In many models the electrochemical behavior of a cell is described using empirically determined current-voltage relations. These are curves valid at a constant temperature for which an applied current can be matched to the total potential over one cell, V_{cell}. An example can be found in figure 4.5. As described in chapter 7 dynamic behavior will cause the cell temperature to change, which leads to the conclusion that a relation describing this curve with a constant temperature cannot be used for a dynamic model. In order to determine the current-voltage relations the following method will be used.

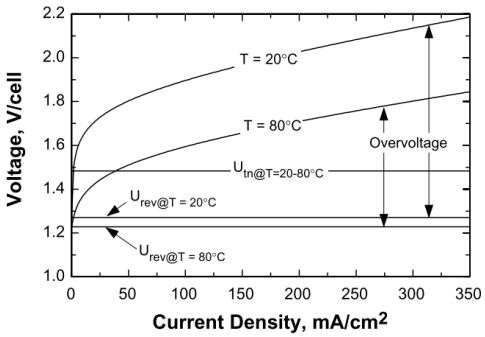

Figure 4.5: A figure of two current-voltage curves at 20 °C and 80 °C, copy from Ulleberg (2003)

The cell potential originates from the reactions and several irreversibilities. The biggest part is the energy needed for the formation of the products, represented by V_{eq}. Others consist of the activation overpotentials η_{act} at the electrodes and so called ohmic potentials IR_{ohm}. These can be determined from the resistances of the related parts and the current density j. The activation- and ohmic potentials are added to the reversible potential so the cell potential can be expressed by the following equation.

$$V_{cell} = V_{eq} + \eta_{act} + IR_{ohm} \tag{4.19}$$

Faradaic efficiency

The amount of generated gas is directly related to the current density. The actual amount of electrons fed to the stack will not pass through every cell because of inherent loss of energy. This can be caused by bypass currents or recombination of product gases in the cell. The amount hydrogen formed is therefore smaller than expected based the amount of electrons fed to the stack (Burnett and Danly, 1979). The faradaic efficiency (often called current efficiency) will be used to describe the fraction of electrons supplied actually leading to produced hydrogen in the outgoing stream.

$$\eta_f = \frac{j^2}{f_1 + j^2} f_2 \tag{4.20}$$

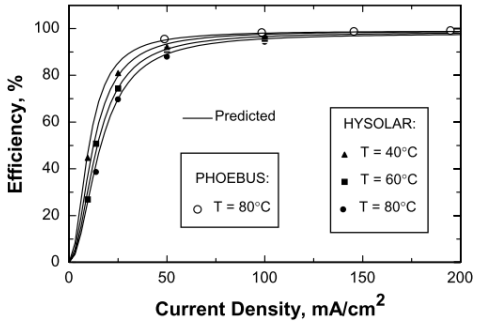

Figure 4.6: A figure of the used faradaic efficiency, ref. from Ulleberg (2003)

The faradaic efficiency is usually a value close to 1 but as the current density drops to the minimal load or if the temperature rises, the loss could increase. The values for f_1 and f_2 have been determined based on an empirical relation given by Ulleberg (2003) and can be found in Table 4.2. The relation was calculated

using a shunt current model by Hug et al. (1992). This empirical correlation is used with the values determined for the HYSOLAR plant (10 kW, 5 bar) to describe the current efficiency.

The rest of the current, not used for the reaction is lost as heat. This fraction is called shunt current. Divisek et al. (1990) states that the main amount of shunt current is lost via the inlet ducts and returned to a cell with a lower potential, leading to low voltage efficiency. Some of the shunt current is not returned to the electrolyzer and used for other unwanted reactions such as corrosion, reverse currents and the generation of invasive gases (O'Brien et al., 2004). The amount lost from the system versus remaining in the system is unknown.

Value	T	f_1	f_2
Unit	°C	$mA^2\ cm^{-4}$	-
	40	150	0.990
	60	200	0.985
	80	250	0.980

Table 4.2: Values for the faradaic efficiency

Open-circuit voltage

V_{eq} is dependent on the species formed during the reaction. As a start the overall reaction can be described using the temperature dependent molar Gibbs energy of formation (Larminie and Dicks, 2013).

$$\Delta\bar{G}_f = \Delta\bar{H}_f - Q = \Delta\bar{H}_f - T\Delta s \tag{4.21}$$

with Gibbs free energy $\bar{G}_f$, enthalpy of formation $\bar{H}_f$ and the amount of energy that is consumed as heat Q, which can be expressed as temperature times the entropy $T\Delta s$.

A relation has been used describing the temperature dependence of the Gibbs free energy. This relation is based on the standard enthalpies and entropies of formation given in Table 4.3 adjusted for temperature using an empirical heat capacity of the reactant and products. The method can be found in Appendix 1 of Larminie and Dicks (2013).

Species	Enthalpy of formation (kJ/mol)
Water (l)	-285.8
Water (g)	-241.8
Hydrogen	0
Oxygen	0

Table 4.3: Enthalpies of formation of half reaction species and standard conditions

The equilibrium potential (also referred to as the open circuit voltage) represents the minimum value at which the reaction can occur. This is the potential at which there is no current running. From the Gibbs free energy the equilibrium potential can be determined.

$$V_{eq} = \frac{\Delta\bar{G}_f}{zF} \tag{4.22}$$

with z being the amount of electrons consumed in the reaction to form one mole of the desired product. Since the model is assumed to operate near standard pressure and the concentration effect is expected to remain small, the concentration and pressure are not taken into account in the Gibbs free energy (Dicks and Rand, 2018).

The net reaction occurring is endothermic. Therefore heat needs to be supplied in an isothermal system to let the reaction run. If at a certain potential the electrical energy supplied is such that no heat is transferred from or to the surrounding (adiabatic process), this is called the thermoneutral voltage V_{tn}.

$$V_{tn} = \frac{\Delta\bar{H}_f}{zF} \tag{4.23}$$

The overall reaction will be endothermic below and exothermic above the thermoneutral voltage. In reality losses to the environment exist, therefore more energy should be supplied to keep the cell at the same temperature. In this thesis this will be referred to as the thermal balancing potential.

Activation overpotential

The activation potential represents the energy required by the charge transfer between the electrode and the chemical species. The relation is strongly dependent on electro-catalytic behavior of the electrodes. The kinetics of the half reactions at the electrodes can be described for the anode and cathode separately by the current dependent Butler-Volmer equation (Hacker and Mitsushima, 2018).

$$j = j_0 \left(\frac{c_R}{c_{R,bulk}} \exp\left(-\frac{\alpha F \eta}{RT} \right) - \frac{c_O}{c_{O,bulk}} \exp\left(\frac{(1-\alpha) F \eta}{RT} \right) \right) \tag{4.24}$$

Here α is the charge transfer coefficient, j_0 the exchange current density, c_R and c_O the concentrations of the reducing and oxidizing components at the electrode and $c_{R,bulk}$ and $c_{O,bulk}$ the concentrations in the bulk of the fluid. The overpotential at an electrode is given by $\eta = V - V_{eq}$ where V is the potential at the electrode. The concentration effect is assumed to be small as long as the current density remains less than about 10% of the smallest limiting current density $j_{l,an}$ or $j_{l,cat}$ (Bard and Faulkner, 2001), so it is left out, leading to the Butler-Volmer equation.

$$j = j_0 \left(\exp\left(-\frac{\alpha F \eta}{RT} \right) - \exp\left(\frac{(1-\alpha) F \eta}{RT} \right) \right) \tag{4.25}$$

If the overpotential is relatively large, though still small compared to the limiting current, eq. 4.25 can be rewritten. For large overpotentials, either positive or negative, one of the two terms becomes negligible and drops out, e.g. η is negative:

$$j = j_0 \exp\left(-\frac{\alpha F \eta}{RT} \right) \tag{4.26}$$

If this is rewritten, a Tafel form equation (4.27) is found from which the overpotential at a certain current density can be determined.

$$\eta = a + b \log(j) \tag{4.27}$$

$$= \frac{RT}{\alpha F} \ln(j_0) - \frac{RT}{\alpha F} \ln(j) \tag{4.28}$$

$$= \frac{2.303RT}{\alpha F} \log(j_0) - \frac{2.303RT}{\alpha F} \log(j) \tag{4.29}$$

Here b is the Tafel slope. To determine the activation potential, the Tafel slopes and exchange current density of both the anode and cathode are determined and then used in the Tafel equation.

Electrode material

Depending on the material and surface structure the properties of the electrode changes. Often the electrode properties are not disclosed by manufacturers and therefore characteristic values are often determined by experiments.

Since the specific properties of the electrodes used in the plant are not known, characteristic values have been derived based on research of the most likely similar electrodes. Wendt and Plzak (1982) have performed experiments to determine electrode kinetics of several materials. For example values for steel blasted nickel electrodes measured at 90 °C and 1000A/m^2 can be found in Table 4.4.

Parameter	Anode	Unit	Cathode	Unit
Charge transfer coefficient α	1.22	K^{-1}	0.55	-
Tafel slope b (@ 90 °C)	59	mV	131	mV
Activation energy E	80	kJ/mol	50	kJ/mol

Table 4.4: Electrode parameters determined from experiments ref. from Wendt and Plzak (1982)

Anode

Charge transfer coefficient & Tafel slope

Wendt and Plzak (1982) have shown that the values for the anodic Tafel slope b_a may not be described by a type of Tafel relation (4.27) but by an equation being only temperature dependent in the exchange current density $j_{0,a}$ term.

$$\eta_a = 2.303 \frac{R}{\alpha_a F} \log\left(\frac{j}{j_{0,a}}\right) \tag{4.30}$$

By doing so the charge transfer coefficient α_a becomes a reciprocal of the temperature instead of a dimensionless number this case. Since the Tafel slope of the anodic activation potentials have been measured to be nearly constant, the anodic Tafel slope $b_a = 0.059$ will be constant for all temperatures.

4

Exchange current density

In order to determine the exchange current density, measurements from Norsk Hydro A.S. (1978a) were used. This patent describes the same or at least similar electrodes present in their current design, among which the NEL A485 stack considered in this research. This patent describes an anodic activation potential η_a = 0.26V at 80 °C and 1000 A/m^2.

From this potential and by rewriting eq. 4.27 the exchange current density can be determined at 80 °C.

$$j_{0,a,80°C} = \frac{j}{\exp\left(\frac{\alpha_a F \eta_a}{RT}\right)} = 0.0397 \text{ A/m}^2 \tag{4.31}$$

The Arrhenius equation (4.33) describes the temperature dependence of reaction rates. The exchange current density is a representation of the reaction rate, the higher the number, the lower the related activation potential. Since all values are known from the patent pre-exponential constant A_a can be determined at 80°C. Then using the pre-expontential factor A_a and the activation energies E_a from Table 4.4 the exchange current densities at other temperatures can be determined. The patent did not mention the activation potentials at all. Therefore the activation energy of a steel blasted nickel electrode has been taken from Wendt and Plzak (1982).

$$A_a = \frac{j_{0,a,80°C}}{e^{\frac{-E_a}{RT}}} \tag{4.32}$$

$$j_0 = A_a e^{\frac{-E_a}{RT}} \tag{4.33}$$

Cathode

Charge transfer coefficient & Tafel slope

Wendt and Plzak (1982) have shown that the cathodic Tafel slope b_c can be described by the Tafel relation.

$$j = j_{0,c} \log\left(2.303 \frac{\alpha_c F \eta}{RT}\right) \tag{4.34}$$

The Tafel slope b_c will therefore be temperature dependent and can been determined using the following equation.

$$b_c = 2.303 \frac{RT}{\alpha_c F} \tag{4.35}$$

Exchange current density

In order to determine the exchange current density, measurements from Norsk Hydro A.S. (1978b) were used. This patent describes the same or at least similar electrodes present in their current design, among which the NEL A485 stack considered in this research. This patent describes an cathodic activation potential η_c = 0.10V at 80 °C and 1000 A/m^2.

From this potential and by solving eq. 4.31 for the cathodic values, the exchange current density can be calculated: $j_{0,c,80°C} = 163.61$ A/m^2.

Similar to the calculation at the anode the pre-exponential constant A_c can be determined at 80 °C. Then using pre-expontential factor A_c and the activation energies E_c from Table 4.4 in eq. 4.33 the exchange current densities at other temperatures can be determined. The patent did not give values for the activation potentials, although it was mentioned that the cost of activation was lower than other known activation methods including noble metals. For consistency the activation energy of steel blasted nickel electrode from Wendt and Plzak (1982) was used .

Anode & cathode

Now that the exchange current density and Tafel slopes have been determined the activation potential of the cathode and anode can be calculated using the following equation.

$$\eta_{act} = b_a \log\left(\frac{j}{(1-\varepsilon_g)j_{0,a}(T)}\right) + b_c(T) \log\left(\frac{j}{(1-\varepsilon_g)j_{0,c}(T)}\right) \tag{4.36}$$

Note that the gas holdup is present in the equation. This assumption is a correction for the fraction of the electrode surface covered by gas rendering it inaccessible for the liquid to react, thereby increasing the current density. In this case the gaseous fraction in the cell ε_g in the electrolyte has been taken as the bubble coverage of the electrode. This has been taken from Abdin et al. (2017), it must be considered that there is a lot of debate around the gas holdup and the effects thereof in liquid electrolyte and on electrodes.

Ohmic potential

As with every electrical circuit, each conducting material has inherent resistances. These ohmic resistances individually add to the potential that has to be applied for hydrogen generation. The potential can be expressed using ohms law.

$$IR_{ohm} = IR_{lye,a} + IR_{sep} + IR_{lye,c} \tag{4.37}$$

Here I is the total current supplied to the stack. Within the cell the electrodes are very good conductors so only the electrolyte and diaphragm resistance are taken into account.

Electrolyte conductivity

The electrolyte resistance in the cell can be determined from the resistivity, the inverse of the effective conductivity and Pouillet's law.

$$R_{lye} = \rho\frac{d}{A} = \frac{d_{eld/sep}}{\kappa_{eff}A} \tag{4.38}$$

Where $d_{eld/sep}$ is the distance between the separator and the electrodes and A the inner diameter of the electrolyzer cell. Here κ_{eff} is the effective conductivity. If bubbles are generated the ions have to travel around the bubbles and therefore travel a longer distance. The parameters of the gas bubbles are not exactly known as already discussed in 2.3.1. Therefore it is hard to calculate the effect of bubbles exactly. Sigrist et al. (1979) have compared several curves to correct the electrical conductivity of the liquid for the dispersion of gas using the gas holdup. For a large particle size-range the Bruggeman equation shown in eq. 4.39 has shown good agreement.

$$\kappa_{eff} = \kappa_{lye}(1-\varepsilon_g)^{\frac{3}{2}} \tag{4.39}$$

with ε_g being the gas holdup, the space in the fluid taken up by the bubbles. Gilliam et al. (2007) have performed experiments and determined the following equation to describe the gas free conductivity κ_{lye} of aqueous KOH. The resulting fit is given in eq. 4.40.

$$\kappa_{lye} = AM_{lye} + BM_{lye}^{2} + CM_{lye}T_{lye} + D\frac{M_{lye}}{T_{lye}} + EM_{lye}^{3} + FM_{lye}^{2}T_{lye}^{2} \tag{4.40}$$

where $A = -2.041$, $B = -0.0028$, $C = 0.005332$, $D = 207.2$, $E = 0.001043$, $F = -0.0000003$

with M_{lye} being the molarity in mol/L and T_{lye} being the temperature of the lye in Kelvin.

Assuming that the inner diameter is equal to the electrode area, eq. 4.38 can be rewritten into eq. 4.41. The potential due to the electrolyte simply becomes as follows. This is determined separately for the anolyte and catholyte because of different gas holdups, compartment size and potentially different current densities.

$$IR_{lye} = j\frac{d_{eld/sep}}{\kappa_{eff}} \tag{4.41}$$

Separator conductivity

The separator is a diaphragm wetted by the electrolyte. The electrolyte is the conducting element in the diaphragm and therefore the ohmic potential related to the separator can be calculated as an expression using the gas-free electrolyte and a correction factor called the MacMullin number N_M.

$$IR_{sep} = \frac{jd_{sep}\mathrm{N_M}}{\kappa_{lye}} \tag{4.42}$$

The separator resistance of a Zirfon separator of 0.5 mm thick consisting of 85wt% ZrO_2 and 15wt% polysulfone in 30% KOH has been measured by Vermeiren et al. (1998). A temperature dependent MacMullin number is determined using the measured separator resistance. The determination of this curve can be found in Appendix C. Using this curve in eq. 4.42 the resistance of the separator can be determined.

Stack degradation

The electrodes in Rjukan are replaced every 8 years due to degradation. This can be attributed to the electrodes becoming less effective over time, which causes the overall potential to increase.

Degradation is usually expressed as a percentage of the total potential per year ζ. Eq. 4.43 has been used to correct for the degradation with stack age a_{stack}.

$$V_{cell,deg} = \frac{a_{stack}\zeta}{100}V_{cell} \tag{4.43}$$

4.2.3. Thermal model

From the outgoing flow and the amount of lye in the compartments the heat capacity of the cell can be determined. If the amount of heat generated or consumed by the reaction, generated by the (over)potentials and the heat losses are known, one can determine the compartment temperature using the lumped thermal capacity. Due to the crossover and large interfacial area between the compartments, it is assumed that the heat is equally divided over the two compartments.

The heat generated will depend on the total current fed to the stack, note that the gaseous heat capacity is not taken into account due to its negligible contribution.

$$\frac{d}{dt}T_{cell} = \frac{\dot{Q}_{tot}}{\sum \bar{c}_{p,L,i}n_{L,i} + c_{p,bp}m_{bp} + c_{p,eld}m_{eld}} \tag{4.44}$$

$$\dot{Q}_{tot} = \dot{Q}_{net} + \dot{Q}_R + \dot{Q}_{pot} + \dot{Q}_{far} - \dot{Q}_{ext} - \dot{Q}_{evap} \tag{4.45}$$

Here $\dot{Q}_{tot}$ is the total heat supplied to the cell, T_{cell} is the temperature of the cell, $\bar{c}_{p,L,i}$ the molar heat capacity of liquid fraction of species i in the two compartments, $n_{L,tot,i}$ the total molar amount of liquid of species i present, $c_{p,bp}$ and m_{bp} the densimetric heat capacity and mass of the bipolar plate, $c_{p,eld}$ and m_{eld} the densimetric heat capacity and mass of the two electrodes. In eq. 4.45 $\dot{Q}_{net}$ is the heat supplied or removed by the in- and outgoing flows, $\dot{Q}_R$ is the reaction heat, the heat contribution due to current supplied for the reaction $\dot{Q}_{pot}$, due to shunt current transformed to heat $\dot{Q}_{far}$, the heat losses to the exterior $\dot{Q}_{ext}$ and the evaporation of water $\dot{Q}_{evap}$.

Net heat in- and outflow

The compartments are operating at temperature T_{cell}, the feed enters the cell at T_{in} and the gases exit at the compartment temperature. Therefore the heat needed to get the feed at the compartment temperature can be expressed.

$$\dot{Q}_{net} = \bar{c}_{p,in}\dot{n}_{L,in}(T_{in} - T_{cell}) \tag{4.46}$$

Reaction heat

The electrical energy consumed when the reaction occurs will not supply all the energy needed. Additional thermal energy is needed from the environment making the reaction endothermic, so the value $\dot{Q}_R$ should be negative. In practice this amount can easily be calculated from the faradaic current density and equations 4.22 and 4.23. The difference in potential represents the heat consumed by the reaction.

$$\dot{Q}_R = \mathrm{I}_{cell}\eta_f(V_{eq} - V_{tn}) \tag{4.47}$$

Heat generation due to ohmic resistance and overpotentials

Heat generation is caused by the (over)potentials inside the cell. This is the heat generated at the electrode, in the electrolyte and the heat generated in the diaphragm.

$$\begin{aligned}\dot{Q}_{pot} &= \dot{Q}_{act} + \dot{Q}_{lye} + \dot{Q}_{sep} \\ &= \mathrm{I}_{cell}\eta_f\eta_{act} + \left(\mathrm{I}_{cell}\eta_f\right)^2\left(R_{a,lye} + R_{c,lye} + R_{sep}\right) && (4.48) \\ &= \mathrm{I}_{cell}\eta_f\left(V_{cell} - V_{eq}\right) && (4.49)\end{aligned}$$

This would effectively result in merging $\dot{Q}_R$ and $\dot{Q}_{pot}$ if V_{eq} in eq. 4.47 is replaced with V_{cell}.

Faradaic heat

Another effect that also adds heat to the cell are the parasitic losses. The electrons not supplied for the reaction, the difference between the total and the faradaic current, will be transformed to heat.

$$\dot{Q}_{far} = \mathrm{I}_{cell}\left(1 - \eta_f\right)V_{cell} \tag{4.50}$$

Heat dissipation

The temperature difference of the stack components and the exterior cause heat to be dissipated, so it cools down the cell. A detailed heat loss model has been developed by Lira Garcia Barros (2019). This model is specifically developed for the NEL electrolyzer focused on in this thesis and will be used to determine the heat losses. The electrical analogy describing the system is given in Figure 4.7.

The model describes determining R_{total}, which involves finding the equilibrium temperature of the gasket surface in each timestep. The conductive, convective and radiative resistances can be determined using material properties, ambient conditions and orientation of the stack. Using eq. 4.51 the heat transfer to the exterior can then be determined. For the detailed explanation of the determination of the heat transfer Lira Garcia Barros (2019) should be consulted.

$$\dot{Q}_{ext} = \frac{T_{stack} - T_{amb}}{R_{total}} \tag{4.51}$$

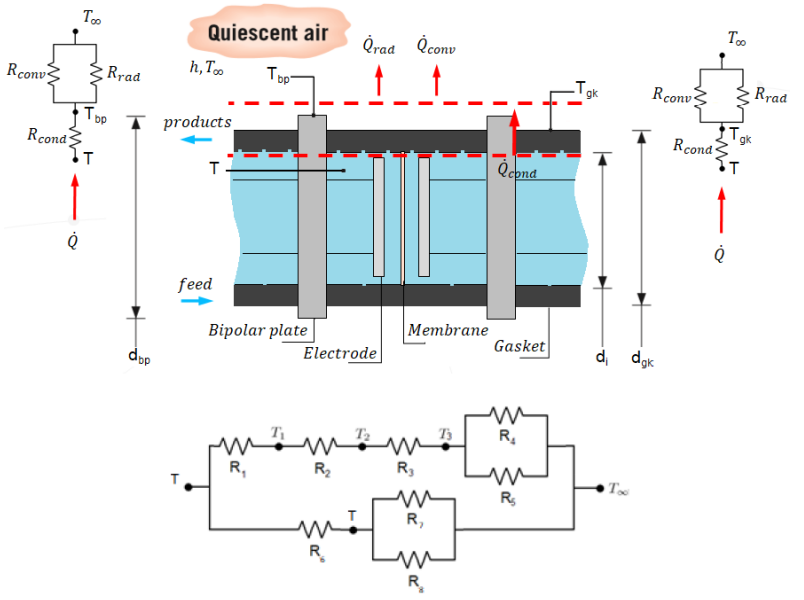

Figure 4.7: Resistance networks describing heat transfer in the stack, copy from Lira Garcia Barros (2019)

Vaporization heat

The last is the fact that water evaporates to keep up the partial pressure of water in the gaseous phase. The heat required for this is the temperature dependent heat of vaporization times the amount of vapor flowing out of the cell.

$$\dot{Q}_{evap} = \dot{n}_{G,out,H_2O}\left(\bar{h}_{G,H_2O} - \bar{h}_{L,H_2O}\right) \tag{4.52}$$

where $\bar{h}_{H_2O}$ is the specific molar enthalpy of water vapor (G) or liquid (L). From eq. 4.44 and 4.45 the temperature of the compartment can be determined. The temperature can be used as input for next iteration.

4.3. Gas-liquid separator

The balance of plant has been modeled in a straightforward way. As mentioned before, the flows from the stack to the gas-liquid separator contain gas and liquid fractions. The two separators are connected by a pipe called the balancing line at the bottom of the vessel to make sure that only liquid will be able to enter the balancing line. The outlet to the pump is in turn attached to this pipe. The pump feeds the lye through a heat exchanger and is then fed back to the stack. From the top of the vessel all gas including water vapor is assumed to be extracted from the system for further processing.

The gas-liquid separators are simple vessels where all flows come together without any active heating or cooling. An amount of liquid is present in the vessel and is represented by the liquid level. The liquid level is the parameter controlling the freshwater valve. If the liquid level drops below a threshold freshwater is fed to the system until the level surpasses a second threshold level. This way the system is kept at a level which ensures sufficient lye flow to feed the cells. The gas-liquid separators at anodic and cathodic side are both modeled separately using the equations in this section.

4.3.1. Mass balance

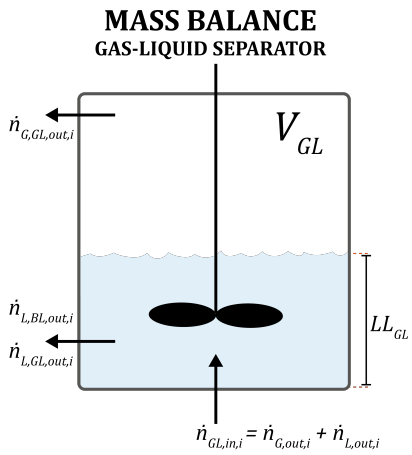

Figure 4.8: Mass balance overview of the gas-liquid separator

From the stack a multi-phase flow will enter the gas-liquid separator, here the mass balance is calculated the same way as in the cell except for the fact that no generation or crossover exists. The material balance is therefore simply defined as the sum of all in- and outgoing flows. The total molar in- or decrease of species i in a compartment in time-step dt is given by the following material balance.

$$\frac{d}{dt}(n_{GL,i}) = \dot{n}_{GL,in,i} - \dot{n}_{GL,out,i} - \dot{n}_{BL,out,i} \tag{4.53}$$

Here $n_{GL,i}$ is the total amount of moles i entering or leaving the gas-liquid separator in one timestep, $\dot{n}_{GL,in,i}$ is the molar inflow of species i from the stack, $\dot{n}_{GL,out,i}$ the molar outflow of species i and $\dot{n}_{BL,out,i}$ the outflow via the balancing line of species i respectively.

The in- and outgoing flows $\dot{n}_{GL,in,i}$ and $\dot{n}_{GL,out,i}$ are split up in a gaseous and a liquid flow. The flow through the balancing line $\dot{n}_{BL,out,i}$ is always liquid.

$$\dot{n}_{GL,in,i} = \dot{n}_{L,GL,in,i} + \dot{n}_{G,GL,in,i} \tag{4.54}$$

$$\dot{n}_{GL,out,i} = \dot{n}_{L,GL,out,i} + \dot{n}_{G,GL,out,i} \tag{4.55}$$

$$\dot{n}_{BL,out,i} = \dot{n}_{L,BL,out,i}. \tag{4.56}$$

For the liquid or dissolved species i the molar in- and outflow of each compartment can be calculated using the following equations.

$$\dot{n}_{L,GL,in,i} = \dot{n}_{L,out,i} \tag{4.57}$$

$$\dot{n}_{L,GL,out,i} = \dot{V}_{L,GL,out} c_{GL,i} \tag{4.58}$$

$$\dot{n}_{L,BL,out,i} = \dot{V}_{L,BL,out} c_{GL,i} \tag{4.59}$$

where $\dot{n}_{L,out,i}$ is the liquid molar flow coming from the stack compartment (see eq. 4.4), $\dot{V}_{L,GL,out}$ the volumetric outflow of the gas-liquid separator to the pump, $\dot{V}_{L,BL,out}$ the volumetric outflow to the other compartment and $c_{GL,i}$ the molar concentration of the concentration in the separator. The concentration in the stack compartments or the other gas-liquid compartment can differ from the concentration in the gas-liquid separator considered. Inflow from these volumes will cause the concentration in the separator to change. This can have an effect on the vapor pressure of water and heat capacity.

The gaseous inflow is equal to the gaseous molar outflow of the stack and can directly be filled in from earlier calculations of $\dot{n}_{G,out,i}$ (see eq. 4.5). The gaseous inflow $\dot{n}_{G,GL,in,i}$ will be bubbled through the liquid column.

$$\dot{n}_{G,GL,in,i} = \dot{n}_{G,out,i} \tag{4.60}$$

The outgoing gaseous fraction will be at saturated water vapor pressure for the gas-liquid separator temperature and electrolyte concentration, the rest is filled with product gas. Using the partial pressure the gaseous molar outflow of species i $\dot{n}_{G,GL,out,i}$ can be described using the ideal gas law.

$$\dot{n}_{G,GL,out,i} = \frac{\dot{V}_{G,GL,out}}{RT_{GL}} p_{GL,i} \tag{4.61}$$

Here $\dot{V}_{G,GL,out}$ is the volume of the gaseous flow leaving the cell in the stack and $p_{GL,i}$ is the partial pressure in the separator of species i.

The partial pressure $p_{GL,i}$ can be determined from the setpoint pressure at which the valve will release the product gases. If the valve would open at 1 atm, automatically the rest of the system would adjust for this pressure, which we will call the gas-liquid pressure p_{GL}. Just like assumed for the stack, only water vapor and the product gas of that compartment are present in the gaseous fraction. Using p_{GL} and by determining the temperature dependent partial pressure of water vapor above the lye p_{GL,H_2O}, the partial pressure $p_{GL,i}$ of the gas can be determined.

$$p_{GL} = p_{GL,i} + p_{GL,H_2O} \tag{4.62}$$

4.3.2. Volumetric balance

The balancing lines allows flow between the two separators to ensure equal anodic and cathodic pressures. The pressure in at the top of both gas-liquid separators p_{GL} is assumed to be equal. If the liquid level on either side is higher, the static pressure at the balancing line connection will be higher. Therefore fluid will flow from there to the separator with the lower liquid level. The two gas-liquid separators are equally sized, therefore half of the difference in volume between the two will be the amount of liquid transferring to the other separator. Keep in mind that in reality this balancing line has a finite flow rate due to wall resistance and inertia.

$$\dot{V}_{L,BL,out} = \frac{1}{2}\Delta V_{L,GL} \tag{4.63}$$

Here $\Delta V_{L,GL}$ is the difference in liquid volume of the two gas-liquid separators.

The liquid volumetric outflow of electrolyte is determined by the pump, balancing line and the volume of demiwater $\dot{V}_{df}$ added to the inlet of the pump.

$$\dot{V}_{L,GL,out} = \frac{1}{2}(\dot{V}_{pump} - \dot{V}_{L,BL,out} - \dot{V}_{df}) \tag{4.64}$$

The amount of moles of each species in the separator $n_{GL,i}$ can be determined by integrating eq. 4.53. This amount can be larger than the capacity of the cell, which causes the excess volume to leave the cell.

$$\dot{V}_{G,GL,out} = \frac{d}{dt}\left(\left(1 - \frac{LL_{GL}}{L_{GL}}\right)V_{GL} - \frac{RT_{GL}}{p_{GL}}\sum n_{G,GL,i}\right) \tag{4.65}$$

Here LL_{GL} and L_{GL} are the liquid level and height in the separator respectively. The liquid level divided by the total height gives us the liquid fraction of the volume, from which the gaseous volume capacity is determined.

4.3.3. Thermal balance

The incoming flows and heat dissipation cause the gas-liquid separator to heat up or cool down.

$$\frac{d}{dt}T_{GL} = \frac{\dot{Q}_{GL,in} - \dot{Q}_{GL,loss} + \dot{Q}_{GL,evap}}{\sum \bar{c}_{p,L,GL,i} n_{L,GL,i}} \tag{4.66}$$

Net heat in- and outflow

The heat required by the inflow to match the separator temperature can be determined using the heat capacity, temperature and molar flow of the flow entering the compartment.

$$\dot{Q}_{GL,in} = \bar{c}_{p,GL,in}\dot{n}_{L,GL,in}(T_{GL,in} - T_{GL}) \tag{4.67}$$

Convective and radiative heat loss

From images of the plant in Rjukan and other NEL plants, an estimate of the outside diameters has been made of the gas-liquid separators. From this it has been estimated that the radius of the separators is 0.86 m and the height is 2.5 m. The surface area of the outside would then be 13.5 m^2 for the sides and 4.65 m^2 for the top and bottom.

The metal the gas-liquid separators are made of has a high thermal conductivity. The resistance is assumed to be low enough to assume $T_{GL} = T_{GL,surface}$. To determine the total heat loss $\dot{Q}_{G,loss}$ of the gas-liquid separator, the convective $\dot{Q}_{GL,conv}$ and radiative heat loss $\dot{Q}_{GL,rad}$ have to be determined.

$$\dot{Q}_{GL,loss} = \dot{Q}_{GL,conv} + \dot{Q}_{GL,rad} \tag{4.68}$$

Convective heat dissipation

The convective heat dissipation at the surface of the gas-liquid separator can be determined from eq. 4.69. A convective heat transfer coefficient $h_{GL,conv}$ is determined and described in Appendix D. Since warm air will rise up parallel to the walls, the convective heat transfer at the walls is expected to be much higher than at the top and bottom. Only the area of the sides $A_{GL,side}$ will be used to calculate the convective heat transfer.

$$\dot{Q}_{GL,conv} = h_{GL,conv} A_{GL} \left(T_{GL} - T_{amb}\right) \tag{4.69}$$

here T_{amb} is the ambient temperature.

Radiative heat dissipation

The radiative heat loss can be determined by using eq. 4.70. Here the total area of the gas-liquid separators A_{GL} is used.

$$\dot{Q}_{GL,rad} = \epsilon_{GL} \sigma_B A_{GL} \left({T_{GL}}^4 - {T_{amb}}^4\right) \tag{4.70}$$

The emissivity of steel varies from very small values to almost 1 depending on the surface. An emissivity of $\epsilon_{GL} = 0.6$ is used.

Vaporization/condensation heat

When the stream from the stack is hotter than the gas-liquid separator, water vapor from the incoming stream will condense supplying heat. The amount that condenses in one timestep is determined by the amount of water vapor in the in- and outflows of the gas-liquid separator. The heat generated is the heat of condensation times the amount of vapor condensed or evaporated. When the incoming stream is cooler than the separator temperature water has to evaporate. Therefore when the amount of vapor leaving is bigger than is entering, the heat generation becomes negative.

$$\dot{Q}_{evap} = (\dot{n}_{G,GL,in,H_2O} - \dot{n}_{G,GL,out,H_2O})(\bar{h}_{G,GL,H_2O} - \bar{h}_{L,GL,H_2O}) \tag{4.71}$$

From eq. 4.66 the temperature of the gas-liquid separator can be determined. The temperature can be used as input for next iteration.

4.4. Pump

The pump is always operated at a constant volumetric flow $\dot{V}_{pump,out}$. Whenever freshwater is fed to the system, the outflow of the gas-liquid separators decreases as can be seen in eq. 4.64.

In the pump the flows from the anodic (GLa) and cathodic (GLc) gas-liquid separators are combined with the demiwater feed (df). All these flows are liquid and the incoming volume is equal to the outgoing volume.

4.4.1. Mass balance

The mass balance can be determined easily as the incoming flow will be equal to the outgoing flow. Because the demiwater feed contains no KOH, the concentration of the outflow of the gas-liquid separators will higher than the concentration of the flow going to the heat exchanger.

$$\dot{n}_{pump,out,i} = \dot{n}_{L,GLa,out,i} + \dot{n}_{L,GLc,out,i} + \dot{n}_{df,i} \tag{4.72}$$

Here $\dot{n}_{L,GLa,out,i}$ and $\dot{n}_{L,GLc,out,i}$ are the outflows of the andodic and cathodic outflows as determined from eq. 4.58. The molar demiwater feed $\dot{n}_{df,i}$ is dependent on the valve controlled by the liquid level of the anodic compartment.

4.4.2. Thermal balance

All flows have their own concentration and temperature. Therefore the temperature of this mixture T_{mix} will be determined using the following equation.

$$T_{mix} = \frac{c_{p,GLa} T_{GLa} \dot{V}_{GLa,out} \rho_{GLa} + c_{p,GLc} T_{Glc} \dot{V}_{GLc,out} \rho_{GLc} + c_{p,df} T_{df} \dot{V}_{df} \rho_{df}}{c_{p,GLa} \dot{V}_{GLa,out} \rho_{GLa} + c_{p,GLc} \dot{V}_{GLc,out} \rho_{GLc} + c_{p,df} \dot{V}_{df} \rho_{df}} \tag{4.73}$$

4.5. Heat exchanger

The flow imposed by the pump will be fed through a plate heat exchanger. A water flow from the nearby river is used to cool the lye. In order to control the lye temperature, the cooling water flow is in- or decreased.

In the model the temperature in the stack is controlled. The desired temperature in the stack is set and based on the actual stack temperature, the PI-controller extracts an amount of heat $\dot{Q}_{cooling}$ from the lye in the heat exchanger n_{HEX}. The temperature of the stack feed can then be determined using the molar heat capacity $\bar{c}_{p,HEX}$. The stack inlet temperature is limited by a 35 °C temperature difference between the in- and outlet temperature.

$$T_{stack,in} = T_{HEX,out} = T_{mix} - \frac{\dot{Q}_{cooling}}{\bar{c}_{p,HEX} n_{HEX}} \tag{4.74}$$

Initial values of the liquid levels, temperatures and a transient current density are fed to the model. All flows are known and therefore the system of equations can be solved. The values calculated are used as input for the next timestep.

5

Model validation

In this chapter the measured data has been used as input for the model and the simulations are compared to the measured data. Based on the differences the simulation results can be put in perspective and potential causes are discussed.

5.1. Initial values and parameters

In order to generate results, initial parameters required to run the model have been estimated. A reflection on some of the parameters and fitted values is shown in Appendix E.

5.2. Timestep

Since the numerical model uses derivatives and integrals to calculate values, the timestep should be set to an appropriate value in order to get relevant results. An important reason to keep timesteps short is the fact that a smaller timestep is required to accurately model the parameters changing in the order of seconds accurately. In order to compare the simulated and measured data, settings listed in Table 5.1 have been used. These have been chosen because smaller steps would significantly increase simulation time and the measured effects are equally well predicted using the timestep chosen. Plots showing the effect of different timesteps on the simulation can be found in Appendix F.

Dataset	Measurement length	Measurement interval	Simulation timestep
1	30 days	≈ 1.5 hours	60 seconds
2	10 days	60 seconds	10 seconds

Table 5.1: Simulation timesteps and dataset information

5.3. Potential

The potential is the most important stack parameter resulting from applying a current. Using the current and temperature as input, the potential is found. The same plot has been made for dataset 1. The potentials in both plots show good agreement. Two differences between the measured and simulated data can be addressed from the graphs.

First it can be seen that the simulation is horizontal at several segments whereas the measured data has a slight slope. This must be caused by changing parameters, either in- or external. A connection seems to be present between the pressure in the gas-liquid separator and the slowly changing measured potential. The pressure in the gas-liquid separators can change if a valve opens, allowing gas to leave the system, or when sudden production is started. A pressure change causes the gas volume present in the lye of the stack and gas-liquid separator to expand or shrink. The rising pressure in the gas-liquid separator would also lead to a pressure rise in the stack. The small decrease of the measured current during those steady-state periods could be attributed to pressure-dependent effects such as smaller ohmic potential due to smaller gas holdup or effect of pressure on the electrode reactions.

The second is the fact that simulation seems to underpredict the potential at higher current densities and overpredict at lower current densities. Several phenomena could cause this problem. The electrolyte resistance could be changing due to a deviation of the simulated gas from the actual gas holdup. Another explanation could be that the Tafel slope of the activation potential is too steep.

5.4. Temperature

An important parameter is the temperature of the stack. Using only current as the input value, the simulated and measured data have been plotted. The same plot has been made for dataset 1.

The temperature of the plant varies during operation and is obviously controlled. The setpoint temperature in Rjukan is changed occasionally for unknown reasons. Since the temperature setpoint of the plant has not been recorded, estimations of setpoints are determined based on the flat line segments. In order to keep the influence of estimation clear, a step increase has been chosen. In reality however, a slower increase could be chosen to prevent unwanted overshoot or other behavior. This could be a reason for the deviation from the model whenever the model setpoint is changed.

Initially a small temperature peak can be seen due to the startup of the model after which the temperature is predicted accurately. The jumps in temperature can be accounted for by the periodic addition of demiwater. During day 3 a drop in temperature can be seen. Here a ramp down from a current density of 1300 A/m^2 to zero occurs which is followed by a ramp up to 900 A/m^2. The current remains zero for roughly 1.5 hours. The model temperature seems to predict the thermal behavior well. A day later another ramp down and up occurs. Here the simulated temperature drop is slightly overpredicted but the time it takes for the temperature to restore to the setpoint temperature is almost the same.

A drop can be seen in the measured temperature between day 15 and 20. This can have several causes, the current is decreased after which the temperature starts to drop. It could be possible that the cooling flow was not adjusted for the new lower current density. The lower current density would lead to less heat generation while the heat dissipation is unchanged, thereby decreasing the cell temperature. Another option is that the operators increased the cooling on purpose to let the cell cool down. In anticipation of the ramp up that follows after the temperature drop, this could be done to prevent temperature overshoot. Since the cooling water flow and temperature have not been measured, validating this statement is not possible.

Just after the setpoint has been set to 70 °C, the measured temperature response is slower than that of the simulated potential. Here it seems that the cooling water flow is larger than necessary. Causing the cell to heat up slower than expected.

Towards the end of dataset 1 the measured temperature is 2 °C lower than the setpoint temperature. The simulation temperature is almost 1 °C below the setpoint. The heat dissipation here is bigger than heat generation causing the cell to cool down. The heat dissipation of the simulation therefore underestimates the actual dissipation. Several effects can be responsible for this difference. This could be caused by an underestimation of the heat-dissipating area and/or heat transfer coefficients. Another reason could be that the ambient temperature of 293.15 K is lower in reality. This could also be the reason for the rise in temperature of the simulation being faster.

5.5. Liquid level

The liquid level in the gas-liquid separators is used to control the fresh feed flow. Whenever the liquid level drops below 32% the demiwater feed valve is fully opened until the liquid level reaches 34%. The maximum demiwater feed rate was determined by comparing the simulated and measured liquid levels, which is shown in Appendix G. The demiwater feed during filling has been determined to be 3.6 m^3/h.

The spike in the simulated liquid level at the start can be attributed to the startup of the model. The stack is initially completely filled with electrolyte which is pushed out as soon as the current is applied at the start of the simulation. The small peaks around the liquid level setpoint of 33.3% are caused by the periodic inflow of demiwater.

Spikes during day 1, 3, 4, 5 and 10 occur in the measured data from the plots. These exceed well above and below the setpoint of the liquid level controller. When comparing these with the measurement data it seems that the gas holdup is only to some extent responsible for the peaks as can be seen during day 3, 4 and 5 and yield both under- and overestimations.

During the peaks at day 1 and 10 the simulated data shows almost no response at all. While the measured

peak at day 1 settles, the current density was increasing. Because this is not shown in the simulation, the large increase in measured data can thus not be attributed to the increase in current density. Instead, a strong relation seems to be present between the pressure in the anodic gas-liquid separator and the liquid level.

A reason for the outflow could be the expansion of the volume in the stack due to a valve opening in the gas-liquid separators. The volume of the gaseous fraction present in the stack expands due to the pressure drop. An abrupt increase in gaseous fraction could lead to the outflow of liquid in the short term. The peaks in liquid level show a strong correlation with a pressure drop. The largest peaks are measured during pressure drops in the anodic gas-liquid separator. Modeling the pressure was only done where necessary and a statement quantifying these effects requires further adjustments and analysis of the model.

The demiwater feed valve control in Rjukan causes the operational parameters to bounce up and down. This makes analysis of the simulation results less convenient. Therefore a simple PI-controller has been developed which controls the liquid inflow such that the liquid level is kept at the setpoint. The demiwater feed rate is still limited to a maximum of 3.6 m^3/h.

5.6. Conclusion

From the comparison between the simulation and the measured data the model performance can be assessed.

The potential shows good agreement. The observed data suggests the simulation to overpredict the potential at low current densities and vice versa. An effect due to pressure seems to be present. The maximum observed difference between the simulation and the measured potential at operating temperatures of 60 °C or higher was 30 mV.

The temperature of the simulation is predicted accurately during operation. The simulated temperature however underestimates the temperature rise time suggesting overlooked heat capacities or increased heat dissipation due to larger heat transfer areas or lower ambient temperatures.

The simulated liquid level seems to show that the simulated gas holdup is larger than the actual holdup. The simulated liquid level is expected to be more sensitive to current density ramps than the actual system. The liquid level in the actual system is influenced by other factors which have not been taken into account. Therefore, the simulation can only predict the liquid level if assuming the pressure in the gas-liquid separators are assumed to be constant.

6

Steady state simulation

Most models found in literature describe steady-state operating points. It should be noted that these points are measured when all varying parameters have settled down. Whenever one of these parameters starts to change, we enter the dynamic domain. In this chapter steady state simulations have been generated using the model. These simulations have been performed using the fresh feed PI-controller to prevent simulation data from bouncing up and down, increasing clarity of the results.

6.1. Current variation

If the temperature setpoint is kept constant at 80 °C and the current is slowly increased making sure that the liquid levels and temperature have time to reach steady state, data points for the full range of currents can be determined.

6.1.1. Heat balance

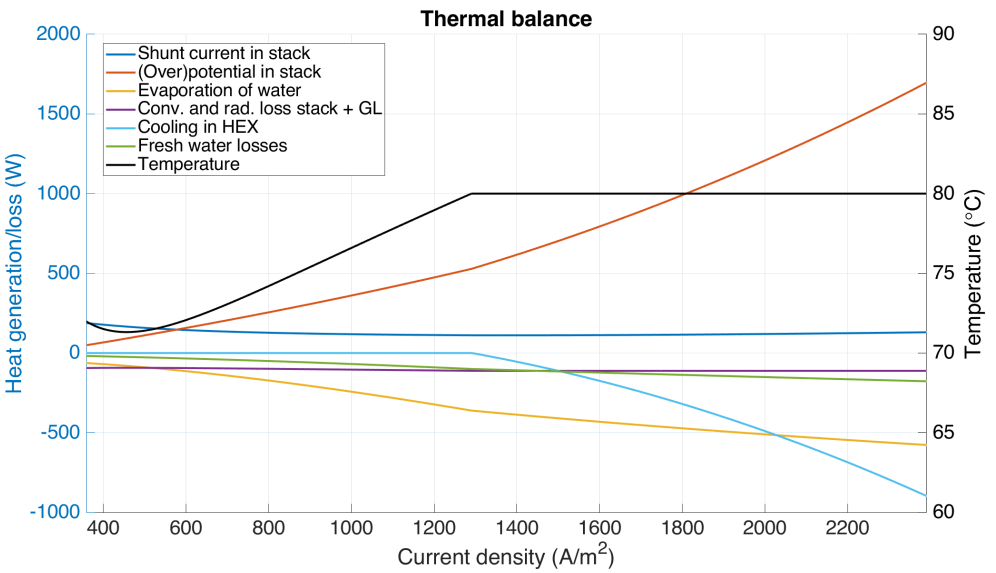

Figure 6.1: The steady state heat balance of a single cell for setpoint temperature 80 °C

Figure 6.1 shows the heat flows and the temperature for a single cell. This figure shows what phenomenon causes heat generation (positive) or loss (negative) at each current density in steady state. As can be seen the cooling only starts at a current density of 1300 A/m^2. Below that point the steady-state temperature is lower than the setpoint of 80 °C. This can mostly be attributed to the decrease in heat generation associated with the reaction. The largest contribution to dissipation is caused by evaporation of water

due to the high vapor pressure of water at 80 °C. The more hydrogen is produced and the higher the temperature, the more water will evaporate and leave the system with the product stream.

Below a current of 1300 A/m^2 the heat generation is not big enough to keep the stack at setpoint temperature. Surprisingly the temperature increases when the current drops below 450 A/m^2. This can be attributed to the increasing contribution of shunt current as was seen from the faradaic efficiency at low current densities. For the shunt current the full potential energy V_{cell} is transformed to heat, whereas for the faradaic current used in the reaction only $V_{cell} - V_{tn}$ is transformed to heat. Although the faradaic current is much larger than the shunt current, the increasing shunt fraction outweighs the overall current drop regarding heat generation.

6.1.2. Potential

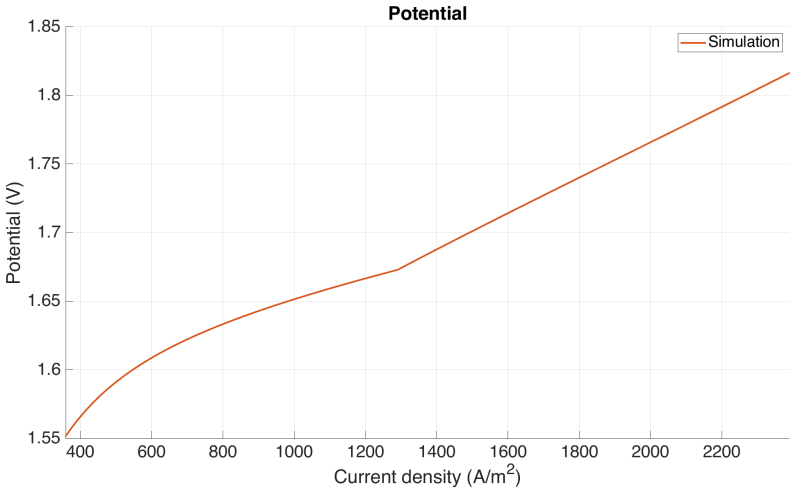

Figure 6.2: The steady state potential of the system for setpoint temperature 80 °C

The potential in Figure 6.2 shows the potential versus the current at the corresponding temperature in Figure 6.1. The potential looks different below 1300 A/m^2 because the steady-state temperature of the stack is varying between 71 and 80 °C. The change in slope is due to the temperature being limited to 80 °C. Above 1300 A/m^2 the temperature does not influence the overall potential anymore. The absolute contribution of the ohmic potential is small compared to the activation potentials, therefore it is expected that the change in the slope of the potential can mostly be attributed to the temperature dependence of the activation potential. The potential has been determined at the highest temperature with $T_{max} = 80$ °C as upper limit and therefore the potentials are the most optimal at the given current.

6.1.3. Electrolyte concentration

When the current is increased the liquid level increases in the gas-liquid separator. The demiwater-feed valve will remain closed and the process consumes water until the desired liquid levels have been reached. The total amount of water in the system changes while the amount of KOH remains equal and therefore the electrolyte concentration starts to vary. This process is elaborated upon in section 8.1.1.

The initial amount of lye in the system in Rjukan and its concentration was unknown. The amount of KOH in the simulation initially is 25 wt% and only water is removed from the system leaving behind the dissolved KOH. During operation the concentration varies between 24 and 33 wt% in extreme cases. The initial amount of lye present in the system determines the absolute amount of mol KOH present. The concentration can be in- or decreased if the concentration or the amount of liquid initially present in the system is changed. The concentration variation due to operation can be seen in Figure 6.3.

A difference in concentration is present at the two sides. The reaction causes water to be consumed at the cathode and produced at the anode. In reality water is transferred through the diaphragm in the cell.

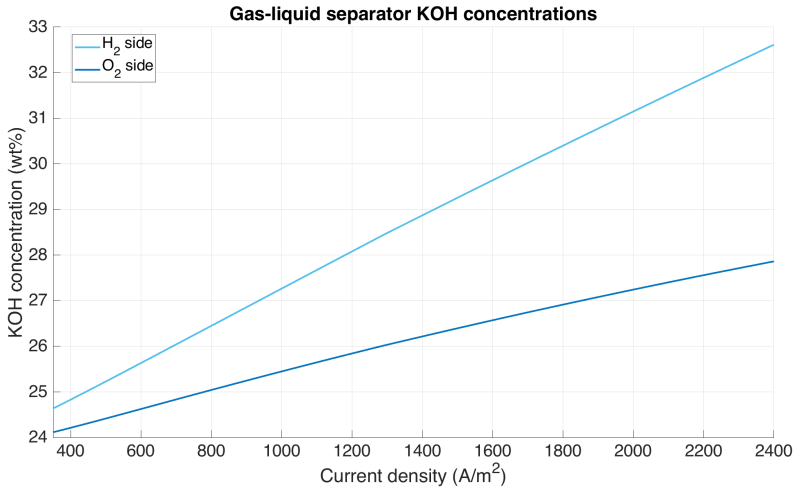

Figure 6.3: The steady state KOH concentration of the system for setpoint temperature 80 °C

However, this is not taken into account in the model. Because water does not cross over through the separator diaphragm, only mixing of the gas-liquid separator outflow and the flow through the balancing line causes the two sides to mix. In reality the concentration difference is expected to be smaller but should still be present.

6.1.4. Efficiency

The model determines the potential based on the current input and time-dependent conditions. The amount of hydrogen produced is also dependent on these conditions. By multiplying the current and stack potential and dividing by the amount of hydrogen flowing out of the system, the energy consumption of the production of 1 Nm^3 (the volume of hydrogen at 0 °C and 1 atm) of hydrogen is known. The energy consumption can be found in Figure 6.4. On the right axis, the energy efficiency is shown. This efficiency has been determined by dividing the enthalpy of formation by the energy consumption. The lowest energy consumption corresponds to the highest efficiency.

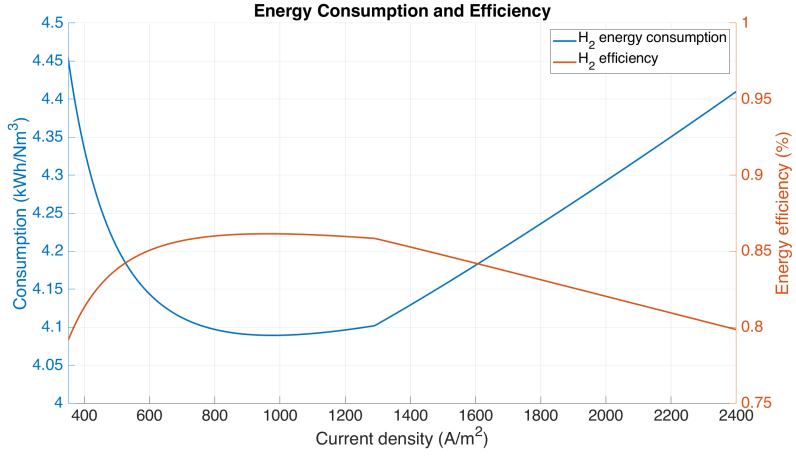

Figure 6.4: The steady state heat balance of the system for setpoint temperature 80 °C

The energy efficiency would be most optimal at 900 A/m^2. The sharp bend in efficiency at 1300 A/m^2 is due to additional heat dissipation of the cooling which causes the temperature to remain constant. The manufacturer of the stack, NEL, lists the energy consumption at 80 °C to be 4.4 kWh/Nm^3 at full load and 3.8 kWh/Nm^3 at minimum load (15%). The latter seems to be incorrect. It should be kept in mind

that the temperature of the simulation at the minimum operating load is 72 °C. The energy consumption in the graph is therefore showing a larger energy consumption than would be the case if the cell would actively be heated to remain at 80 °C.

6.2. Temperature variation

Whenever the operating temperature is changed, many parameters in the system change. The change of steady-state parameters are shown in this section.

6.2.1. Current potential curves

In Figure 6.5 the current-potential curve is shown for different temperatures.

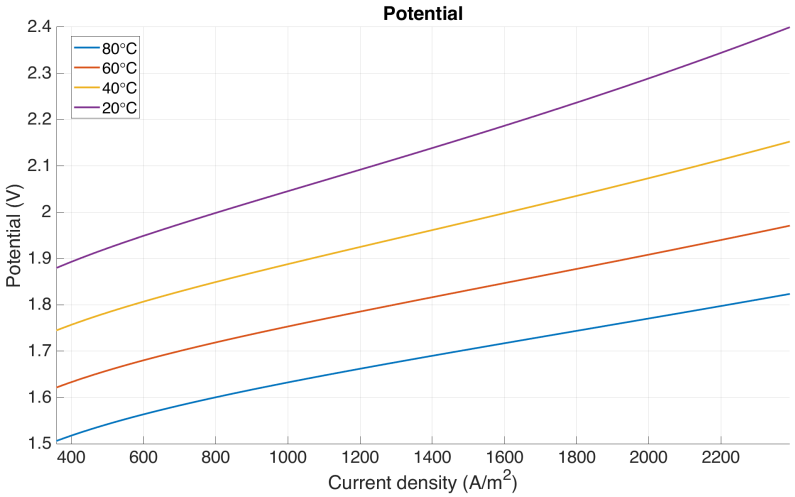

Figure 6.5: Current-potential curves from the minimum to full load at temperatures 20, 40, 60 and 80 °C

It can be seen that the temperature has a large influence on the potential. The simulation of 20 °C shows the effect of the gas holdup on the electrolyte resistance very clearly. The slope is expected to remain constant at higher current densities. Due to the large influence of the resistivity of the electrolyte at low temperatures and an increasing gas holdup, the slope is increasing.

6.2.2. Heat balance

A simulation has been performed to show the heat balance when varying the temperature at a constant current density. This heat balance is shown in Appendix H.

6.3. Maximum load overview

A simulation has been performed at full load and maximum operational temperature. In Table 6.1 the properties of the steady-state flows shown in Figure 6.6 have been listed. For the determination of the gas volume a pressure of 1 atm has been used. In reality these pressures in the system are assumed to be between 101 and 130 kPa.

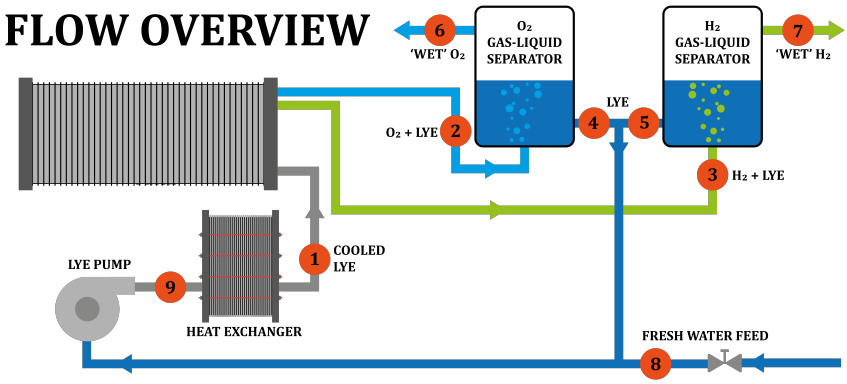

Figure 6.6: Overview of flows in the modeled system

Stream number	1	2	3	4	5
H_2 (g) [kg/s]	0	0	0.01184	0	0
O_2 (g) [kg/s]	0	0.09398	0	0	0
H_2O (g) [kg/s]	0	0.02235	0.03514	0	0
H_2O (l) [kg/s]	2.823	1.495	1.165	1.349	1.311
KOH (aq) [kg/s]	1.155	0.577	0.577	0.521	0.634
Gas volume [m^3/s]	0	0.526	0.986	0	0
Liquid volume [L/s]	3.16	1.68	1.35	1.52	1.52
Fraction G/L [%]	0.00%	99.68%	99.86%	0.00%	0.00%
Temperature [K]	331.40	353.15	353.15	352.00	351.70
Liquid conc. [wt%]	29.03%	27.86%	33.14%	27.85%	32.58%

Stream number	6	7	8	9
H_2 (g) [kg/s]	0	0.01184	0	0
O_2 (g) [kg/s]	0.09398	0	0	0
H_2O (g) [kg/s]	0.02185	0.03469	0	0
H_2O (l) [kg/s]	0	0	0.162	2.823
KOH (aq) [kg/s]	0	0	0	1.155
Gas volume [m^3/s]	0.521	0.979	0	0
Liquid volume [L/s]	0	0	0.16	3.19
Fraction G/L [%]	100.00%	100.00%	0.00%	0.00%
Temperature [K]	352.00	351.70	298.15	348.60
Liquid conc. [wt%]	0.00%	0.00%	0.00%	29.03%

Table 6.1: Mass/heat balance for a complete electrolyzer with a stack of 230 cells operated at 5000 A and 80 °C

7

Dynamic behavior simulation

The parametric response of the system is determined and shown in this section. To determine dynamic results several current ramps have been modeled. The situations that have been simulated are listed below.

1. Instantaneous ramp up to 100% from low load (15%) steady-state operation
2. Instantaneous ramp down to 15% from full load (100%) steady-state operation
3. Instantaneous ramp up to 100% from cold status

The model was allowed to settle down to minimize the effects of startup of the model in situation 1 and 2. The timestep is 1 second and the ramp occurs happens at t = 1550 min. Situation 3 shows the behavior from complete cooldown to full load.

The manufacturer of the cell claims that a ramp rate of 10%/min is possible. In order to assess this claim, situation 1 and 2 have also been performed while using the maximum ramp rate. The plots and analysis describing this event are shown in Appendix I.

7.1. Situation 1: Ramp up from low load

The results of this simulation can be found in Figure 7.1 and 7.2. The cell is operated in steady state at 750 A. The temperature is nearly 72 °C. Once the ramp up to 5000 A occurs the parameters in the system start to change. Pay extra attention to the time span of each plot as the response time varies per parameter.

7.1.1. Thermal effects

The thermal balance shows an increase in heat generation associated with the increased potential in Figure 7.2b. Because the gas production is increased significantly the energy lost to evaporation increases immediately. When the temperature rises the evaporative heat dissipation increases even more. After 90 minutes the temperature peaks at 83 °C. The heat dissipation to the exterior shows an increase as the temperature rises. The cooling shows that the temperature control starts once the temperature is above the setpoint temperature, which is reached after 40 minutes. The demiwater feed heat dissipation starts after more than 500 minutes. This is the point where the liquid level has returned to the setpoint, see Figure 7.2a.

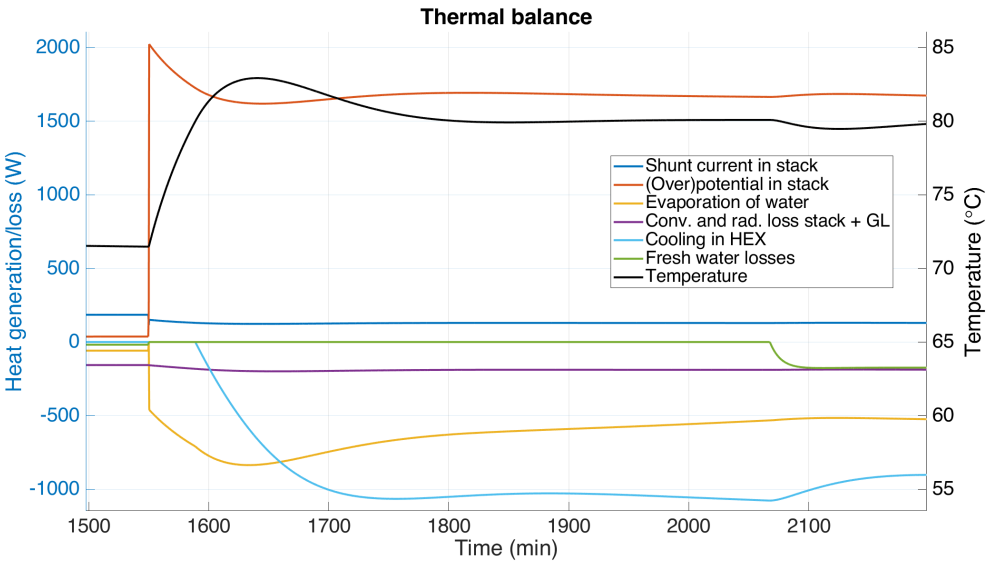

Figure 7.1: The response of the heat balance for a ramp up from 15% to 100% load

7

7.1.2. Mass effects

The liquid level in Figure 7.2c increases to almost 80% in 25 seconds. This can be attributed to the rise in gas holdup causing the gaseous fraction shown in Figure 7.2e to rise. It takes the consumption of water by the reaction over 500 minutes to reduce the liquid level in the gas-liquid separator to the threshold level of 33% as can be seen in Figure 7.2a. The consumption of water causes the electrolyte concentration to increase while the liquid level drops. This effect can be seen in Figure 7.2f. Just after ramp up the potential is high, but soon drops as the temperature settles. The slight changes in potential over time can also be noticed in the energy consumption, which is expressed as the energy consumption over the hydrogen outflow of the system, in Figure 7.2d.

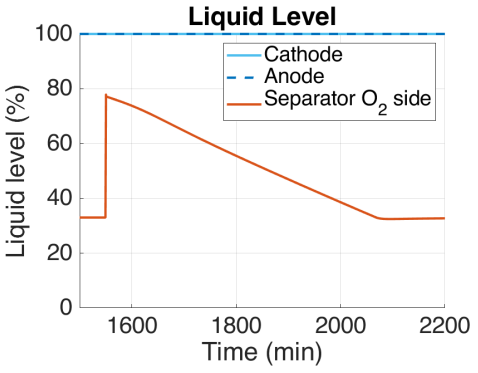

(a) Liquid level response of stack compartments and the anodic gas-liquid separator

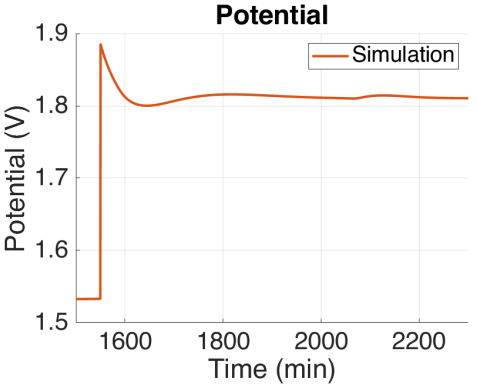

(b) Potential response

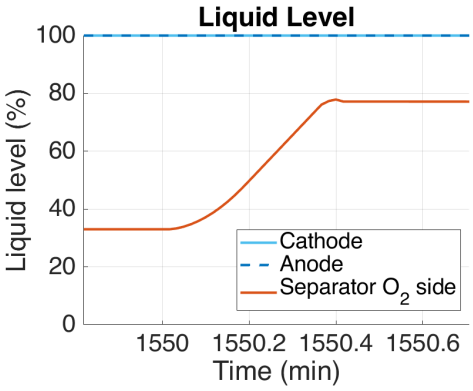

(c) Zoom in on the liquid levels

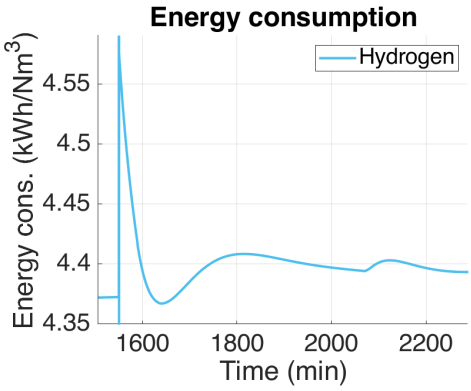

(d) The energy consumption per Nm^3 outflow of hydrogen

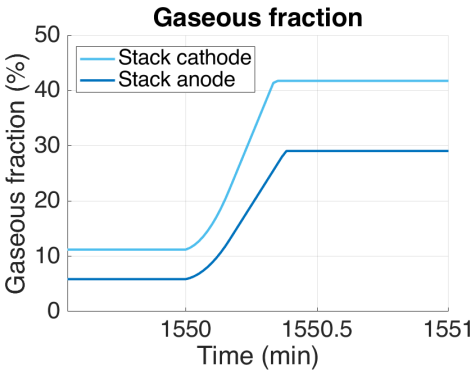

(e) The response of gaseous fraction in the cell

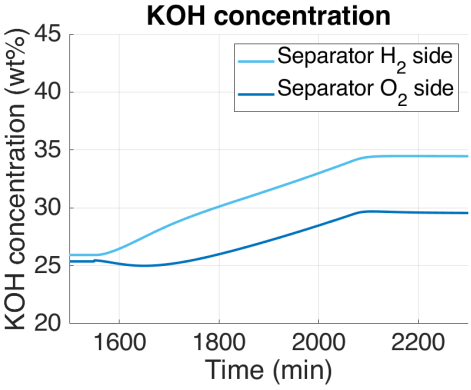

(f) The response of concentration in the cell compartments

Figure 7.2: Simulated parameters of the system for a ramp up from from 15% to 100% load

7.2. Situation 2: Ramp down from full load

The cell is operated in steady state at 5000 A. The temperature is 80 °C. Then the current is suddenly decreased to 750 A. The results from this simulation can be found in Figure 7.3 and 7.4.

7.2.1. Thermal effects

The heat due to the potential in Figure 7.4b decreases while the heat generation due to shunt current increases. Heat dissipation due to evaporation falls due to the smaller amount of gas produced and to a smaller extent the temperature drop. Cooling induced by the demiwater added to refill the system causes the temperature to drop to 66 °C after 100 minutes. After the liquid level has been restored the heat generation due to shunt current becomes dominant. The temperature will start to approach the steady-state temperature given in Figure 6.1. The cooling flow responds quite slow, which can be attributed to the slow response of the temperature controller.

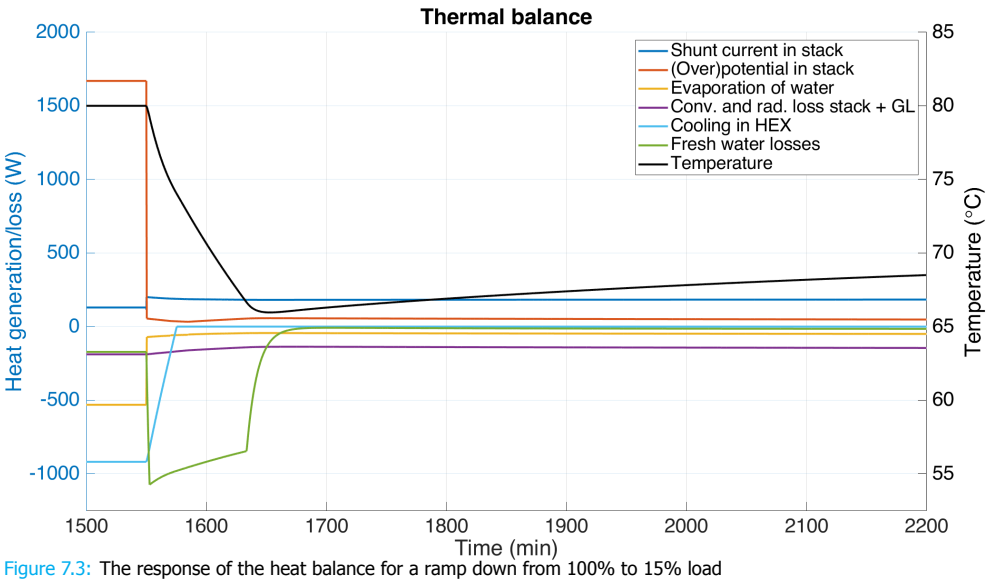

Figure 7.3: The response of the heat balance for a ramp down from 100% to 15% load

7

7.2.2. Mass effects

The liquid column in the stack collapses and the liquid levels in the stack compartments drop. Assuming that no lye can flow back into the stack from the gas-liquid separators, the lye levels of the anodic and cathodic stack compartment are restored after 20 and 35 minutes respectively. As long as the liquid level was not restored, lye did not flow out. The separator liquid levels in Figure 7.4a decrease to a minimum of 4% after 35 minutes. If backflow was possible, lye from the separators would fill the void in the stack. The gas-liquid separator would then be fully drained if the void created by the gas holdup drop in the stack is larger than the volume of the lye in the gas-liquid separator. In the case considered, the gas-liquid separators would be fully drained. Figure 7.4e shows the decrease in gaseous volume due to the inflow of lye. The gaseous fraction in the compartments becomes constant after some time, which is the amount of gas present in the lye due to the new steady-state gas holdup. The liquid level drop in the anodic compartment is smaller due to a smaller gas holdup before ramp down but the level is also restored faster due to the reaction producing water at the anode and consuming at the cathode. Therefore, the slopes of the liquid levels in Figure 7.4c are different. The liquid level drop of the gas-liquid separators slows down once the anodic compartment is full. The liquid flowing from the anodic compartment to the anodic gas-liquid separator flows to the cathodic gas-liquid separator via the balancing line. The separator liquid levels start to increase once both stack compartments have been filled. The separator liquid levels in Figure 7.4a are restored after 100 minutes. The addition of demiwater causes the electrolyte concentration to drop as can be seen in Figure 7.4f. The lower reaction rate causes the dilution and concentration in the stack to decrease, which leads to a smaller concentration difference once the simulation settles.

The energy consumption in Figure 7.4d shows a combined effect of a changing potential and the outflow of hydrogen. The sharp rise in energy consumption can be attributed to a decrease in the outflow of hydrogen, which outweighs the drop in potential. From this peak energy consumption starts to drop due to a decreasing potential. Then a sharp drop can be observed, which can be attributed to a larger outflow of hydrogen: By refilling the cathodic compartment extra hydrogen is already being pushed out of the compartment. Once the lye flow from the (refilled) anodic compartment starts, half of that lye is flowing to the cathodic separator via the balancing line. Therefore the liquid level is dropping less fast, suddenly allowing more hydrogen to leave the cell. Once the liquid level of the cathodic compartment is restored, except for the produced hydrogen no extra hydrogen is pushed out of the stack compartment. The outflow of hydrogen is still higher than the production, since the separators refilling cause additional gas to be pushed out. Only after the separators have refilled, an amount of hydrogen flows out equal to the reaction production. The energy consumption will settle as the potential settles.

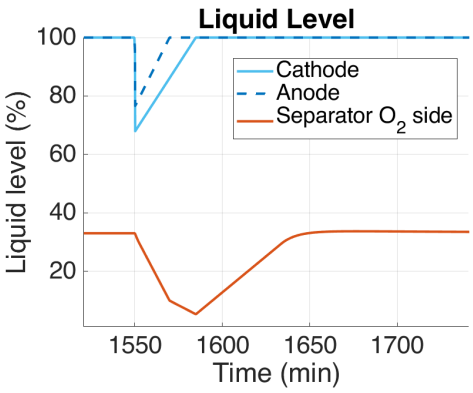

(a) Liquid level response

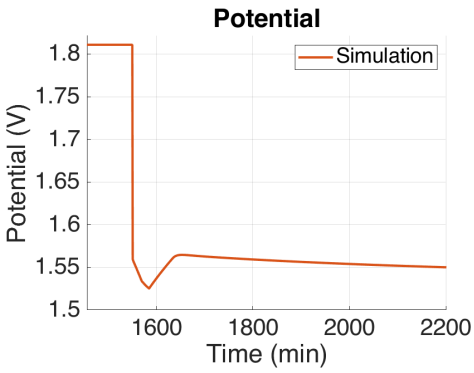

(b) Potential response

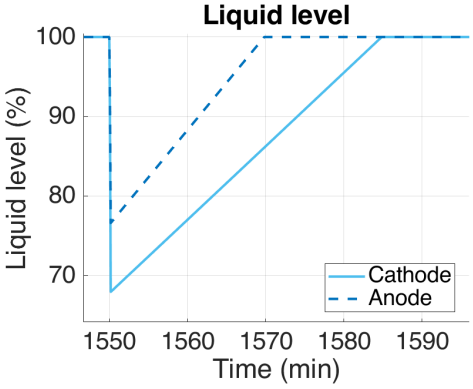

(c) Zoom in on the liquid levels

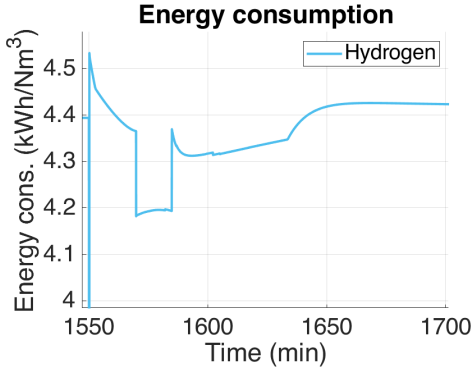

(d) The energy consumption per Nm^3 outflow of hydrogen

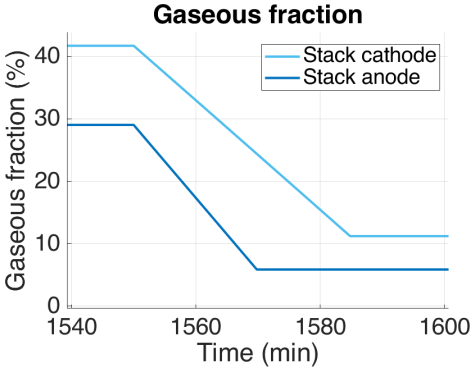

(e) The response of gaseous fraction in the cell

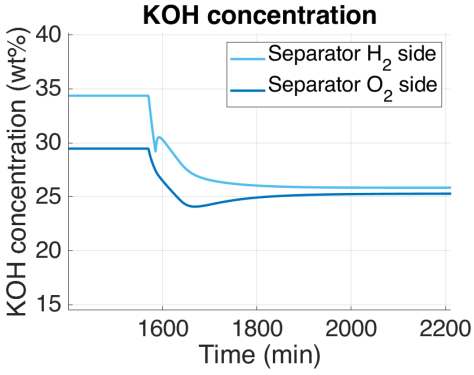

(f) The response of concentration in the cell compartments

Figure 7.4: Simulated parameters of the system for a ramp down from 100% to 15% load

7.3. Situation 3: Ramp up from cold status

The results of this simulation can be found in Figure 7.5 and 7.6. The cell is initially turned off and at a temperature of 20 °C. The initial liquid level in the gas-liquid separator is 25%. The stacks are completely filled with lye initially.

7.3.1. Thermal effects

The thermal balance in Figure 7.5 shows a large increase in heat generation associated with the increased potential in Figure 7.6b. Because the gas production is increased significantly while the temperature rises the energy lost to evaporation increases. The heat dissipation to the exterior increases and heat generation due to shunt currents decreases with temperature. After 230 minutes the temperature peaks at 83 °C. The cooling starts once the temperature is above the setpoint temperature after 185 minutes. The demiwater feed starts after 700 minutes when the liquid levels are back to the setpoint.

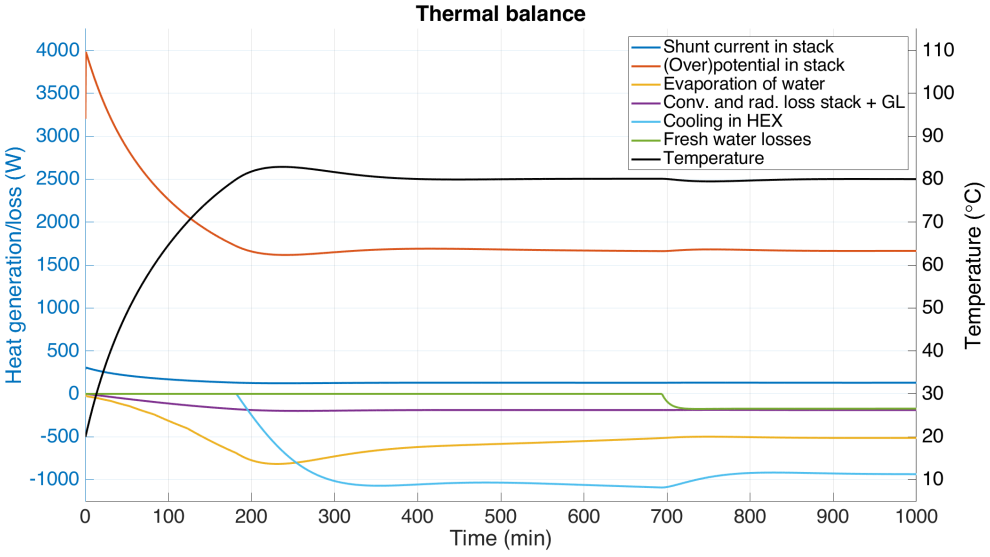

Figure 7.5: The response of the heat balance for a full ramp up from complete cooldown, 0% to 100% load

7.3.2. Mass effects

The liquid level in Figure 7.6c increases from 25% to 84% in 30 seconds. The increase of the gaseous fraction in Figure 7.6e consists fully of the gas holdup. As the temperature rises, the potential and the associated energy consumption drop. The consumption of water by the reaction takes 700 minutes to reduce the liquid level in the gas-liquid separator to the threshold level of 33.3% as can be seen in Figure 7.6a. By then the demiwater feed is started to keep the separator at the setpoint liquid level. The consumption and production of water at the cathode and anode cause the electrolyte to concentrate and dilute respectively. This leads to a concentration difference as can be seen in Figure 7.6f.

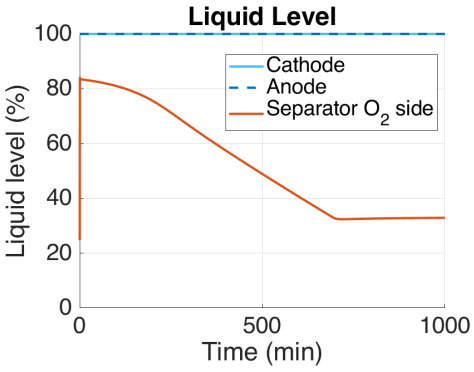

(a) Liquid level response

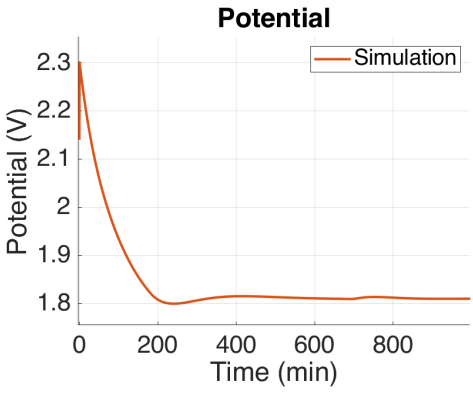

(b) Potential response

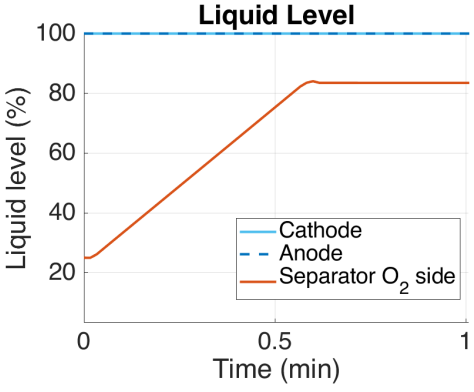

(c) Zoom in on the liquid levels

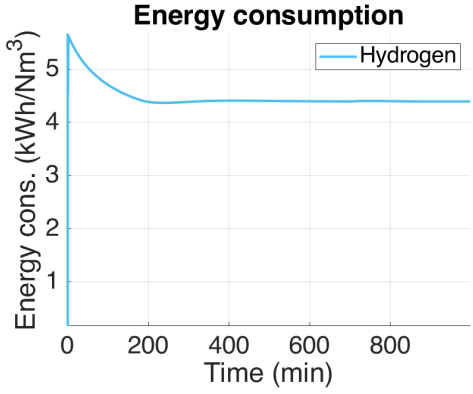

(d) The energy consumption per Nm^3 outflow of hydrogen

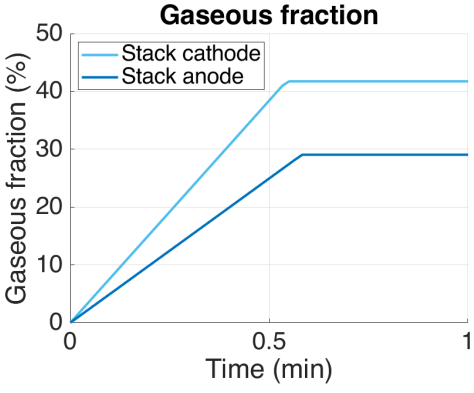

(e) The response of gaseous fraction in the cell

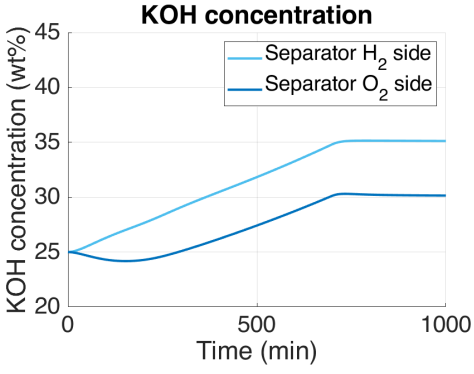

(f) The response of concentration in the cell compartments

Figure 7.6: Simulated parameters of the system for a ramp up from complete cooldown, 0% to 100% load

8

Discussion & Conclusions

The model has been validated and transient simulations have been shown in the previous chapter. In this chapter, the resulting limitations of the system will be addressed. The research questions have been answered and are summarized in the conclusions.

8.1. Flexibility limitations

The behavior of a stack being operated transiently is displayed in the previous chapters. These plots show the parametric response of transient operation. Limiting phenomena and underlying causes are discussed in this section. Potential risks involved with flexible operation are the following:

- Overflowing gas-liquid separators; this would result in the flow of electrolyte to downstream equipment designed to handle gaseous flows.
- Draining gas-liquid separators; this could cause a direct connection between the gaseous fractions of the anodic and cathodic separator via the balancing line. This could lead to mixing hydrogen and oxygen as well as damage to the pump.
- Local overheating; this could result in increased corrosion and/or damage to equipment or parts of the stack such as the electrodes.
- Dryout in the top of the cell; this could lead to increased gas crossover.
- A pressure difference between the anodic and cathodic compartment; this could result in damage to the diaphragm as well as increased lye crossover. The increased crossover contains dissolved gas which could result in transferring too much hydrogen to the oxygen.

The parametric change is further elaborated upon. Phenomena that could lead to any of the hazards listed above are determined based on the simulations. The behavior leading to limitations is described below.

8.1.1. Liquid level

The liquid levels are largely influenced by the gas holdup in the stack. Currently the equation for anodic and cathodic gas holdup described by Haug et al. (2017) has been used as the average holdup for the compartment. The basis for this assumption was explained. From the very preliminary comparison in Appendix J it seems like the simulated gas holdup overestimates the actual holdup but more research is required to assess if this value is correct. If the gas holdup used in this research is close to the actual value, the liquid level would form the biggest limitation for flexible operation.

The effect of a sudden current density increase while operating at steady state (1) has been depicted in Figure 8.1. When the current increases, gas production will start or increase on either side of the diaphragm. Since the compartments are filled with lye, the bubbles push the lye out of the compartment until the steady-state gas holdup is reached. The lye from the stack is pushed into the gas-liquid separators, increasing the liquid level (2). Once the steady-state gas holdup has been reached, the liquid levels in the gas-liquid separators will decrease due to the consumption of water by the process (3). After a while, the system settles and steady state will be reached (4).

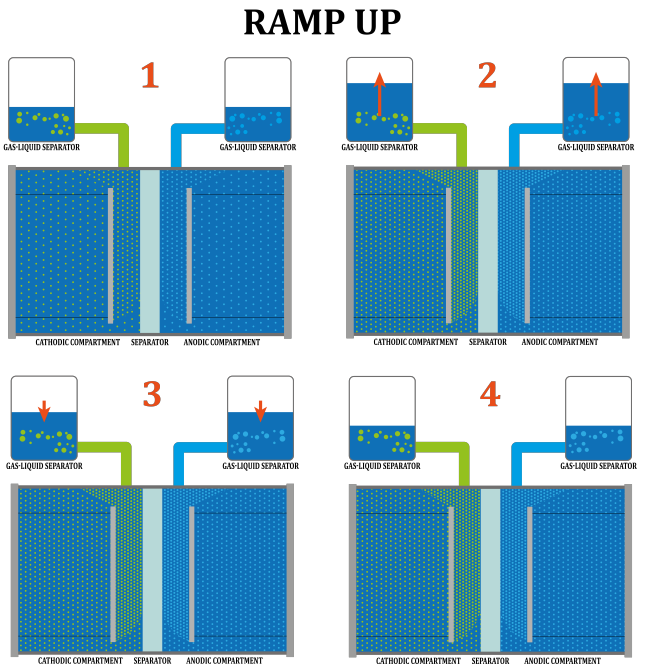

Figure 8.1: The effect in the stack and gas-liquid separator due to a ramp up event

During ramp up, a risk occurs of overflowing of the gas-liquid separators. This should be prevented as it could damage other equipment. In the stack, the generated volume of gas is larger in the cathodic compartment. Therefore, due to inertia of the lye inside the stack, unequal pressures could occur between the anodic and cathodic compartment, which could be harmful to the diaphragm.

The effect of a current drop during steady-state operation (1) has been depicted in Figure 8.2. Whenever a ramp down occurs the gas production decreases or stops and the gas holdup will decrease. The lowered gas holdup causes the liquid level in the stack to drop (2). Slowly the liquid level will restore while the gas-liquid separators are drained by the pump (3). Once the liquid level is restored in the stack, the gas-liquid separators will restore to the regular levels (4). Note that the decrease in gas holdup causes a larger liquid fraction to be present in the stack during steady state operation. The total volume of lye in the system has to increase by adding demiwater to keep the liquid levels the same as before ramp down.

The pump is connected at the center of the balancing line between the two compartments. A safety risk occurs when the liquid level drops below the connection to the balancing line. If that happens the pump could suck gasses out of both separators forming explosive mixtures in the balancing line and pipe to the pump. After a ramp down the liquid levels in the stack compartments differ. This can be attributed to different gas holdups before the collapse of the liquid columns. This could cause a pressure difference over the diaphragm causing increased risk of crossover or rupture of the diaphragm. Dryout of the separator at the top of the stack could lead to the same problems.

The volumes of the gas-liquid separator should be designed to be large enough to prevent overflowing or draining completely during current ramps. Another option is to design the control of the system such that the ramp rate will remain low enough to prevent the separators from flooding or draining completely. The maximum allowable ramp rate is dependent on many parameters, such as dimensions, maximum load, safety considerations, and setpoints of the system. If a liquid level in the separators of 4% is considered safe, according to the simulation the NEL A485 electrolyzer could be ramped up from 0 to 100% without problems.

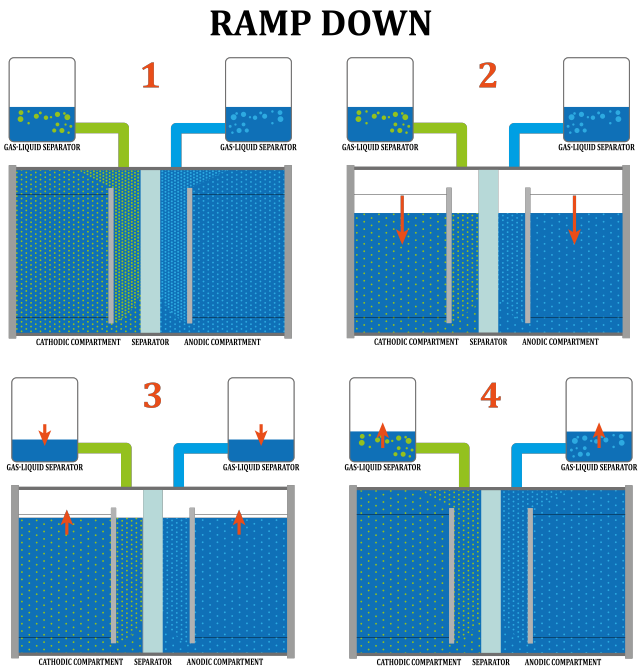

Figure 8.2: The effect in the stack and gas-liquid separator due to a ramp down event

From preliminary calculations, shown in Appendix K, based on the measured liquid level drops in the gas-liquid separators during ramp down, the volumetric outflow of the stack could be determined. It was found that the volumetric outflow of the gas-liquid separators is roughly 4 times larger than the pump circulation. Therefore it is expected that liquid flows back into the stack. If this is the case, the risk where dry-out could pose problems is omitted. Then only the liquid level in the gas-liquid separators is the limiting value.

8.1.2. Temperature

Another important parameter is the temperature of the stack. Since the response of the temperature is pretty slow, it can be controlled accurately. This is the case as long as the cooling duty required to keep the system from overheating does not exceed the limitations of the heat exchanger and restrictions on stack inlet conditions.

The efficiency is lower when the stack is operating at lowered temperatures. At lower temperatures, the internal resistance is higher and more heat will be generated. The stack, therefore, tends to heat up if operated at low temperatures. Naturally, at high current densities, heat generation is larger leading to faster heat up. Evaporative losses increase significantly with larger hydrogen flows and higher temperatures. The temperature increase is therefore dampened at elevated temperatures.

As the stack gets older the potential increases due to stack degradation. This causes heat generation to increase. Over time the stack will be able to heat up faster which could be beneficial if fast heat up is desired. However, it might be possible that operation at high current densities will cause the heat generation to become higher than the maximum cooling capacity. Since operation at temperatures higher than 80 °C could lead to several problems, this should be prevented.

8.2. Conclusions

A dynamic thermal model has been developed in this research. The development of a model describing alkaline electrolysis based on physical equations is challenging yet insightful. The concept of using physical equations to describe properties of electrolyzers has proven to be a successful method for the determination of electrochemical, mass, and thermal behavior. The simulation yields results in line with measurements of an actual large scale electrolyzer.

The research questions have been answered in the research and are summarized below:

- *How are operational parameters of alkaline hydrogen production, such as potential and temperature, influenced by transient operation?*

  When looking at the main research question it is desired to know how transient operation influences alkaline hydrogen production. From the analysis in the previous chapters, the behavior of an alkaline stack becomes clear. As can be seen from the simulations in Model validation and Dynamic behavior simulation, many parameters change when transiently operated. The effects on most of the parameters are limited to relatively slow changes and can often be controlled to remain within safe limits. The liquid levels and concentration deserve attention as these seem to be influenced most by transient operation. The concentration varies over time because demiwater is used to control the liquid levels in the system. Since the concentration could influence corrosion this is a parameter to keep in mind. The liquid level forms a direct limitation regarding ramp times and is elaborated upon below.

- *What factors are limiting fast ramp times?*

  It has been shown that the most critical factor limiting fast ramp times are the liquid levels in the system. These are mainly influenced by the fast changes in gas holdup in the stack. These changes could cause gas-liquid separators to flood or be drained during operation. This could be mitigated if the design is accommodated to these liquid volume fluctuations, leaving the potential dryout of the stack as a problematic issue. The response of the liquid levels is fast compared to the temperature. The temperature in the electrolyzer can be controlled by varying the cooling. This is partly due to the slow response of the temperature as well as the dampening effects seen at elevated temperatures. The inflow of freshwater and the evaporation of water consume an increasing amount of heat at higher temperatures and currents. The temperature could become a limiting factor if the available cooling is insufficient.

- *Should ramp rates be limited?*

  It has been shown in the simulations that large current ramps do not completely drain or flood the gas-liquid separators. However during ramp down the liquid level almost dropped to zero. The effects on the gas-liquid separator of in- or decreased liquid levels differ per system and should be assessed in greater detail based on the system design. The effects on the electrode and diaphragm due to decreased liquid levels in the stack are unknown and could be harmful. However, measurements have shown high ramps without any reported problems. If the liquid levels in the gas-liquid separators are monitored and kept at safe levels, there is no reason that ramp rates should be limited in this plant.

- *How will ramp rates influence operational parameters, thermal behavior in particular?*
  &
- *Should the stack be allowed to cool down during low-load operation or be actively heated?*

  It has been shown that the startup from a cooled down situation takes roughly 3 hours before the operational temperature of 80 °C is reached. If a lower load is used the heat up time will increase. Nearly no active heating is needed if the stack is operated at its minimal operating load. When operating at the minimum load (15%) the stack will remain within 10 °C of the operational temperature, mainly due to the heat generated by an increased fraction of shunt current. When ramping up a cell operated at low load, it takes roughly 35 minutes to get the cell at the operational temperature. Technically there is no reason to keep the cell heated to operational temperature. However keeping the cell at elevated temperatures, especially if cheap residual heat from nearby industry is used, would lead to lower electricity consumption.

9

Recommendations

9.1. Recommendations

Gas holdup in the stack largely determines the rise in liquid levels. Since the gas holdup has such a large influence, the model requires good estimations to generate reliable results. The values in this research seem to be overpredicting the actual gas holdup. The data has too few points where the influence of controllers or other parameters was known such that this statement can be validated. Therefore, further research is required to determine reliable gas fractions.

The operational pressure affects the volume of the gas formed in the stack. When the pressure is increased, especially at lower pressures, the gas holdup decreases and the effects on the liquid levels in the stack become smaller. This would allow for smaller (potentially cheaper and less hazardous) designs, smaller ohmic losses, and less evaporation of water. The effect on the liquid levels due to pressure changes can then be analyzed. In further research, the influence of pressure should therefore be analyzed.

All crossover through the separator diaphragm is assumed to be zero in this research, except the OH^- required by the reaction. In reality water, KOH, hydrogen, and oxygen cross over through the diaphragm and via the mixing of flows. In alkaline electrolysis usually the gas purity of both outflows is monitored to prevent explosion hazards. From preliminary calculations, the amount of indirect crossover of hydrogen and oxygen via mixing is very small except at very low loads (« 15% load). This can probably be attributed to the small circulation flow. Further research should include crossover on larger stacks with small flows to address the influence of the large interfacial area between the anodic and cathodic compartments.

The faradaic efficiency has now been taken from experiments of a small scale plant. The faradaic efficiency becomes most important at lower loads. In further research, the source of losses should be determined and a better estimation of where the losses are transformed to heat. By doing so, a better estimation of the heat loss at low current densities can be made.

References

Abdin, Z., Webb, C. J., and Gray, E. M. A. (2017). Modelling and simulation of an alkaline electrolyser cell. *Energy*, 138:316–331.

Afif, A., Radenahmad, N., Cheok, Q., Shams, S., Kim, J. H., and Azad, A. K. (2016). Ammonia-fed fuel cells: A comprehensive review.

Amores, E. and Carreras, C. (2014). Influence of operation parameters in the modeling of alkaline water electrolyzers for hydrogen production. 9.

Bard, A. J. and Faulkner, L. R. (2001). *ELECTROCHEMICAL METHODS - Fundamentals and Applications*, volume 2. John Wiley & Sons, 2nd edition.

Boissonneau, P. and Byrne, P. (2000). Experimental investigation of bubble-induced free convection in a small electrochemical cell. *J. Appl. Electrochem.*, 30(7):767–775.

Brauns, J. and Turek, T. (2020). Alkaline water electrolysis powered by renewable energy: A review. *Processes*, 8(2).

Burnett, J. and Danly, D. (1979). Current bypass in Electrochemical Cell Assemblies.pdf.

Caspersen, M. and Kirkegaard, J. B. (2012). Modelling electrolyte conductivity in a water electrolyzer cell. *Int. J. Hydrogen Energy*, 37(9):7436–7441.

Churchill, S. W. and Chu, H. H. (1975). Correlating equations for laminar and turbulent free convection from a vertical plate. *Int. J. Heat Mass Transf.*, 18(11):1323–1329.

Churchill, S. W. and Usagi, R. (1972). A general expression for the correlation of rates of transfer and other phenomena. *AIChE J.*, 18(6):1121–1128.

David, M., Alvarez, H., Ocampo-Martinez, C., and Sánchez-Peña, R. (2020). Dynamic modelling of alkaline self-pressurized electrolyzers: a phenomenological-based semiphysical approach. *Int. J. Hydrogen Energy*.

Davis, R. E., Horvath, G. L., and Tobias, C. W. (1967). The Solubility and Diffusion coefficient of Oxygen in Potassium Hydroxide Solutions. *Electrochim. Acta*, 12(May 1965):287 – 297.

Dicks, A. L. and Rand, D. A. J. (2018). *Fuel Cell Systems Explained*. Wiley.

Divisek, J., Mergel, J., and Schmitz, H. (1990). Advanced Water Electrolysis and Catalyst Stability under Discontinuous Operation. 15(2):105–114.

Douglas, T. G., Cruden, A., and Infield, D. (2012). Development of an ambient temperature alkaline electrolyser for dynamic operation with renewable energy sources. *Int. J. Hydrogen Energy*, 38(2):723–739.

Funk, J. E. and Thorpe, J. (1969). Void Fraction and Current Density Distributions in a Water Electrolysis Cell. *J. Electrochem. Soc.*, 116(48).

Gilliam, R. J., Graydon, J. W., Kirk, D. W., and Thorpe, S. J. (2007). A review of specific conductivities of potassium hydroxide solutions for various concentrations and temperatures. *Int. J. Hydrogen Energy*.

Götz, M., Lefebvre, J., Mörs, F., McDaniel Koch, A., Graf, F., Bajohr, S., Reimert, R., and Kolb, T. (2016). Renewable Power-to-Gas: A technological and economic review. *Renew. Energy*, 85:1371–1390.

Guban, D., Muritala, I. K., Roeb, M., and Sattler, C. (2019). Assessment of sustainable high temperature hydrogen production technologies. *Int. J. Hydrogen Energy*.

Hacker, V. and Mitsushima, S. (2018). *Fuel Cells and Hydrogen*. Susan Dennis.

Haug, P., Kreitz, B., Koj, M., and Turek, T. (2017). Process modelling of an alkaline water electrolyzer. *Int. J. Hydrogen Energy*, 42(24):15689–15707.

Haynes, W., Lide, D., and Bruno, T. (2014). *CRC Handbook of Chemistry and Physics*. CRC Press, Boca Raton, 95 edition.

Henao, C., Agbossou, K., Hammoudi, M., Dubé, Y., and Cardenas, A. (2014). Simulation tool based on a physics model and an electrical analogy for an alkaline electrolyser.

Hine, F. (1985). *Electrode Processes and Electrochemical Engineering*. Plenum Press, New York.

Huber, M., Dimkova, D., and Hamacher, T. (2014). Integration of wind and solar power in Europe: Assessment of flexibility requirements. *Energy*.

Hug, W., Bussmann, H., and Brinner, A. (1993). Intermittent operation and operation modeling of an alkaline electrolyzer. *Int. J. Hydrogen Energy*, 18(12):973–977.

Hug, W., Divisek, J., Mergel, J., Seeger, W., and Steeb, H. (1992). Highly efficient advanced alkaline electrolyzer for solar operation. *Int. J. Hydrogen Energy*, 17(9):699–705.

IEA (2019). The Future of Hydrogen for G20. Technical report, International Energy Agency.

Junginger, M. and Louwen, A. (2020). *Technological Learning in the Transition to a Low-Carbon Energy System*. Brian Romer.

Kasahara, S. (2011). Water Electrolysis. In Yan, X. L. and Hino, R., editors, *Nucl. Hydrog. Prod. Handb.*, pages 83–97. Taylor and Francis Group.

Kellermann, H., Jüttner, K., and Kreysa, G. (1998). Dynamic modelling of gas hold-up in different electrolyte systems. *J. Appl. Electrochem.*, 28(3):311–319.

Kreysa, G. and Kuhn, M. (1985). Modelling of gas evolving electrolysis cells. I. The gas voidage problem. *J. Appl. Electrochem.*, 15(4):517–526.

Larminie, J. and Dicks, A. (2013). Appendix 1: Change in Molar Gibbs Free Energy Calculations. In *Fuel Cell Syst. Explain.*, volume 1, pages 391–394.

Le Bideau, D., Mandin, P., Benbouzid, M., Kim, M., and Sellier, M. (2019). Review of necessary thermophysical properties and their sensivities with temperature and electrolyte mass fractions for alkaline water electrolysis multiphysics modelling. *Int. J. Hydrogen Energy*, 44(10):4553–4569.

Lira Garcia Barros, R. (2019). *Flexibility study of an alkaline water electrolysis process*. PhD thesis, Technische Universiteit Eindhoven. PDEng thesis. - Confidential.

Lüke, L. and Zschocke, A. (2020). Alkaline Water Electrolysis: Efficient Bridge to CO2-Emission-Free Economy. *Chemie-Ingenieur-Technik*, 92(1-2):70–73.

MacMullin, R. B. and Muccini, G. A. (1956). Characteristics of porous beds and structures. *AIChE J.*, 2(3):393–403.

Martínez, M. J., Shimpalee, S., and Van Zee, J. W. (2009). Measurement of MacMullin Numbers for PEMFC Gas-Diffusion Media. *J. Electrochem. Soc.*, 156(1):B80.

Milan, P., Wächter, M., and Peinke, J. (2013). Turbulent character of wind energy. *Phys. Rev. Lett.*, 110(13):1–5.

Millet, P. and Grigoriev, S. (2013). Water Electrolysis Technologies. In *Renew. Hydrog. Technol. Prod. Purification, Storage, Appl. Saf.*, pages 19–41. Elsevier B.V.

Mills, A. (2013). *Basic Heat and Mass transfer*. Pearson Education Limited, second edition.

Norsk Hydro A.S. (1978a). Method for preparing active anodes for electrochemical processes, particularly for manufacture of hydrogen. UK patent - GB1565040A.

Norsk Hydro A.S. (1978b). Method for preparing active cathodes for electrochemical processes. UK patent - GB1548147A.

O'Brien, T., Bommaraju, T., and Hine, F. (2004). *Handbook of Chlor-Alkali Technology - Volume I: Fundamentals*.

Olivier, P., Bourasseau, C., and Bouamama, P. B. (2017). Low-temperature electrolysis system modelling: A review. *Renew. Sustain. Energy Rev.*, 78(January 2016):280–300.

Oluf Jensen, J. (2008). Pre-investigation of water electrolysers. Technical report.

Ortner, A. and Totschnig, G. (2019). The future relevance of electricity balancing markets in Europe - A 2030 case study. *Energy Strateg. Rev.*, 24(January):111–120.

Rostrup-Nielsen, J. R. and Rostrup-Nielsen, T. (2002). Large-scale hydrogen production. *Cattech*, 6(4):150–159.

Sánchez, M., Amores, E., Rodríguez, L., and Clemente-Jul, C. (2018). Semi-empirical model and experimental validation for the performance evaluation of a 15 kW alkaline water electrolyzer. *Int. J. Hydrogen Energy*.

Santos, D. M., Sequeira, C. A., and Figueiredo, J. L. (2013). Hydrogen production by alkaline water electrolysis. *Quim. Nova*, 36(8):1176–1193.

Schalenbach, M., Lueke, W., and Stolten, D. (2016). Hydrogen diffusivity and electrolyte permeability of the Zirfon PERL separator for alkaline water electrolysis. *J. Electrochem. Soc.*, 163(14):F1480–F1488.

Schalenbach, M., Zeradjanin, A. R., Kasian, O., Cherevko, S., and Mayrhofer, K. J. (2018). A perspective on low-temperature water electrolysis - Challenges in alkaline and acidic technology. *Int. J. Electrochem. Sci.*, 13(2):1173–1226.

Schmid, R. (2018). Ptx - when electrolysis is coming..., presentation.

Seibel, C. and Kuhlmann, J. W. (2018). Dynamic Water Electrolysis in Cross-Sectoral Processes. *Chemie-Ingenieur-Technik*, 90(10):1430–1436.

Sequeira, C. A., Santos, D. M., Šljukić, B., and Amaral, L. (2013). Physics of Electrolytic Gas Evolution. *Brazilian J. Phys.*, 43(3):199–208.

Sigrist, L., Dossenbach, O., and Ibl, N. (1979). On the conductivity and void fraction of gas dispersions in electrolyte solutions. *J. Appl. Electrochem.*, 10(2):223–228.

Tilak, B. V., Lu, P. W. T., Colman, J. E., and Srinivasan, S. (1981). Electrolytic Production of Hydrogen. In *Compr. Treatise Electrochem.*, pages 1–104.

Tjaden, B., Cooper, S. J., Brett, D. J. L., Kramer, D., and Shearing, P. R. (2016). On the origin and application of the Bruggeman correlation for analysing transport phenomena in electrochemical systems. *Curr. Opin. Chem. Eng.*, 12:44–51.

Trinke, P., Haug, P., Brauns, J., Bensmann, B., Hanke-Rauschenbach, R., and Turek, T. (2018). Hydrogen crossover in PEM and alkalinewater electrolysis: Mechanisms, direct comparison and mitigation strategies. *J. Electrochem. Soc.*, 165(7):F502–F513.

Ulleberg, Ø. (2003). Modeling of advanced alkaline electrolyzers a system. *Hydrog. Energy*, 28:21–33.

Ursúa, A. and Sanchis, P. (2012). Static-dynamic modelling of the electrical behaviour of a commercial advanced alkaline water electrolyser. *Int. J. Hydrogen Energy*, 37(24):18598–18614.

VDI-GVC (2010). *VDI Heat Atlas*. Springer Berlin Heidelberg, second edition.

Vermeiren, P., Adriansens, W., Moreels, J. P., and Leysen, R. (1998). Evaluation of the zirfon® separator for use in alkaline water electrolysis and Ni-H2 batteries. *Int. J. Hydrogen Energy*.

Wang, M., Wang, Z., Gong, X., and Guo, Z. (2014). The intensification technologies to water electrolysis for hydrogen production – A review. *Renew. Sustain. Energy Rev.*, 29:573–588.

Wendt, H. and Plzak, V. (1982). Electrocatalytic and Thermal activation of Anodic Oxygen- and Cathodic Hydrogen- evolution in AWE.

Zarghami, A., Deen, N. G., and Vreman, A. W. (2020). CFD modeling of multiphase flow in an alkaline water electrolyzer. *Chem. Eng. Sci.*, 227:115926.

Zeng, K. and Zhang, D. (2010). Recent progress in alkaline water electrolysis for hydrogen production and applications. *Prog. Energy Combust. Sci.*, 36(3):307–326.

A

Net species transport example

When the electrolyzer is operated, next to hydrogen, oxygen and water vapor, lye is flowing out of the stack. Liquid forms a very small volumetric fraction of the flow leaving the electrolyzer. 485 Nm^3/h of hydrogen gas is produced if an electrolyzer with lye at 30 wt% KOH and 80°C is operating at full load. The partial pressure of water vapor $p_{H_2O} \approx 0.3$ bar for water as can be seen from figure A.1, where 1 mm Hg ≈ 133 Pa. If the total pressure is 1 atm, then $p_{H_2} \approx 0.7$ bar results for hydrogen from equation 4.6. The total volume of gas leaving the cell can be determined assuming that half the amount of hydrogen of oxygen is formed. A simple calculation shows us that if the pump operates at a circulation rate of 11.5 m^3/h, the volume fraction of the liquid in the outgoing stream of the stack is very small.

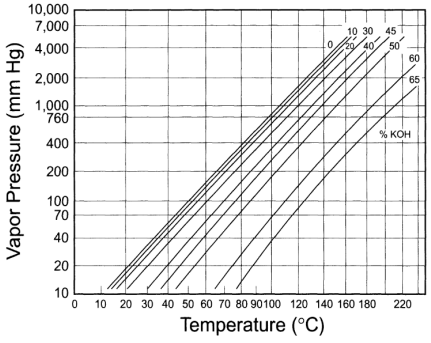

Figure A.1: The vapour pressure of H_2O at certain temperatures and concentrations (Ulleberg, 2003)

$$\dot{V}_{G,out} = 1.5\frac{485}{0.7} = 1040 \qquad \dot{V}_{in} = 11.5 \tag{A.1}$$

$$\text{Vol\% of liquid in } \dot{V}_{out} = \frac{\dot{V}_{\text{in}}}{\dot{V}_{out}} \approx \frac{11.5}{1040 + 11.5} = 1.1 \text{ vol\%} \tag{A.2}$$

Note that the outgoing lye stream is smaller than the incoming lye feed due to water consumption and evaporation. Also the 485 Nm^3/h is at 0°C while the actual temperature would lie around 80°C. Therefore in reality the liquid fraction will be even smaller. The value determined here is just a rough estimation to show the order of magnitude.

B

Gas holdup rationale

The gas holdup of large scale hydrogen production has not been researched extensively. An estimation has to be made for the amount of gas and liquid in the stack. Therefore a maximum gas holdup is determined empirically for each compartment at a certain current density as described by Haug et al. (2017). The experimental setup used to determine the relations consisted of a zero-gap electrolyzer with a distance between the separator and the bipolar plate of 15 mm. Although this setup does not have a gap between the electrode and separator, the space behind the electrode is similar to the cells in Rjukan. Moreover the electrolyte used was 28.6 wt% KOH at 80°C which determines the limiting gas holdup according to Kreysa and Kuhn (1985).

The experiment has shown that the gas holdup did not vary at different feed flow rates. From the theory by Kellermann et al. (1998) it follows that the gas holdup has reached its limiting gas holdup in this case. The flow velocity should have been even higher to reduce the gas holdup. Since the upward flow velocity in the cell in Rjukan is much smaller than the experiments by Haug et al. (2017) and the height of the cell is much larger, the lye in Rjukan will reach the limiting gas holdup at a low height.

In reality it is expected that the gas holdup between the electrode and diaphragm is higher than the holdup in the volume behind the electrode. The gas holdup in each of these volumes is subject of discussion. The bubble size is expected to be small causing the buoyancy to be small. Therefore, circulation inside the stack compartment is expected to circulate bubbles behind the electrode.

Assuming the limiting gas holdup to be reached at a low height in the cell, this value is be taken as the average gas holdup. The anodic and cathodic compartments produce different amounts of gas and therefore the gas holdup equation for these compartments is different.

C

Membrane properties

According to MacMullin and Muccini (1956) the MacMullin number is defined as

$$N_M = \frac{R_{sep}}{R_{lye}} \tag{C.1}$$

where R_{sep} is the resistance of the porous medium saturated with the electrolyte and R_{lye} is the resistance of the electrolyte itself. According to Martínez et al. (2009) it can also be described as the ratio between the tortuosity and the porosity which depend on properties of the medium considered.

The separator resistance of a Zirfon separator in 30% KOH has been measured by Vermeiren et al. (1998). This is a diaphragm of 0.5 mm thick consisting of 85wt% ZrO_2 and 15wt% polysulfone. A temperature dependent MacMullin number can be determined from eq. C.2 using the measured separator resistance shown in Figure C.1 and the properties of the separator and electrolyte used for the experiment.

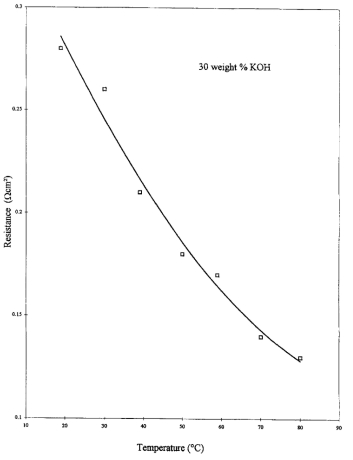

Figure C.1: Separator resistance in 30% KOH solutions, copy from Vermeiren et al. (1998)

$$N_M(T) = \frac{R_{sep}\kappa_{lye}}{L_{sep}} \tag{C.2}$$

The curve shown in Figure C.1 is represented by the following curve (Lira Garcia Barros, 2019).

$$R_{sep} = A_{sep} \cdot T(^\circ C)^2 + B_{sep} \cdot T(^\circ C) + C_{sep} \tag{C.3}$$

with $A_{sep} = 2.11454 \times 10^{-5}$

$B_{sep} = -0.004676135$

$C_{sep} = 0.366916305$

If eq. C.3 is substituted in eq. C.2 a temperature dependent MacMullin number is found.

D

Convective heat dissipation

The gas liquid separator sides can be seen as vertical plates if the curvature is neglected. For gases with Prandtl number (Pr) close to 1 a transition to a turbulent boundary layer is said to occur at a Grashof number (Gr) of approximately 10^9 (Mills, 2013). A Prandtl number function Ψ can be determined from Churchill and Usagi (1972). Then using a correlation for turbulent flow over a plate with a sharp leading edge the average Nusselt number $\overline{\mathrm{Nu}}_L$ can be determined (Churchill and Chu, 1975). In this formula the Rayleigh number Ra_L will be used which can be determined from the Grashof and Prandtl number.

$$\mathrm{Ra}_L = \mathrm{Gr}_L \mathrm{Pr} = \frac{\beta \Delta T g {L_{GL}}^3}{\nu^2} \mathrm{Pr} \tag{D.1}$$

$$\Psi = \left(1 + \left(\frac{0.492}{Pr}\right)^{9/16}\right)^{-16/9} \tag{D.2}$$

$$\overline{\mathrm{Nu}}_L = 0.68 + 0.670 \left(\mathrm{Ra}_L \Psi\right)^{1/4} \left(1 + 1.6 \times 10^{-8} \mathrm{Ra}_L \Psi\right)^{1/12} \tag{D.3}$$

Using the Nusselt number, the heat transfer coefficient h_{GL} can be determined as given below.

$$h_{GL,conv} = \frac{\kappa_{air}}{L_{GL}} \overline{\mathrm{Nu}}_L \tag{D.4}$$

E

Reflection on simulation results

Parameters

Before commenting on the simulated behavior, it should be noted that the model was built to simulate the behaviour of the plant in Rjukan. Therefore the parameters used were either known or an estimation was made. This estimation was made based on literature, NEL presentations and website, patents and experienced people at Nouryon. If any of the parameters in Chapter 3 are changed, the system behaviour will change. Most of the changes will only cause small changes on the behaviour, some are more sensitive. The estimates with a relatively large impact are discussed below.

The dimensions and material of the stack components are not all known. The electrodes for example are modeled as solid 5 mm thick slabs. The thickness has not been measured and no data could be found. From experts estimation the most reliable value was obtained and has been used. If the electrodes are less thick the internal volume of the stack increases. If the volume increases the amount of liquid pushed to the gas-liquid separator during ramp up and refill time during ramp down will increase. The same holds for the perforations in the plate, due to the lack of details these holes have not been taken into account.

As seen from the example above, the choice for a value of one parameter can lead to changes in the system elsewhere. The stack described is a commercial system and not all information is known exactly. The absolute values gained from this research are therefore far from generally applicable and of less importance compared to the transient effects observed. The insights in phenomena and the learnings are representative for many more electrolyzers.

Fitting has been used to set the temperature controller. The controller setpoints were estimated from the input data and using those the response has been determined. By doing so the thermal response of the model has been fitted to the thermal response of the plant in Rjukan. Other fittings are the values used to determined the MacMullin number and the patents and paper (Norsk Hydro A.S., 1978a,b; Wendt and Plzak, 1982) used for the determination of the exchange current density. The faradaic efficiency and gas holdup were also determined using experimental data.

Faradaic efficiency

It has been assumed that all of the energy that is not used for the formation of hydrogen is transformed to heat. This assumption causes the steady state cell temperature to increase when operating at loads below 1250 A. In reality it is unknown what ratio of the current is lost by parasitic currents or by the reverse reaction by recombination of hydrogen and oxygen. Although in both cases heat is generated, the latter happens outside the cell and should therefore not add to the cell temperature.

Liquid level in stack

In this research it is assumed that no lye can flow back from the gas-liquid separators into the stack. From the detailed dataset 2 however it has been calculated that the rate of decrease in liquid level after a ramp down is much larger than the pump can drain the compartment. No signs of dry-out could be seen in the form of increased potentials after a ramp down. These findings would suggest that liquid is flowing back into the stack. The results in this research of the creation of a void in the stack after ramp down therefore showcases a the worst case scenario.

The liquid level drop in the stack due to ramp-down is restored by the inflow. This inflow is fixed at the capacity of the pump, 11.5 m^3/h or a little less than 14 ml/s per cell. The pump determines the time it takes for the lye to be refilled. The main reason of the flow being so small is that the feed channels have a very small diameter to reduce shunt currents. These small channels are the most likely bottleneck and therefore increasing the pump power without increasing the channel size would lead to increased energy use.

Another effect is that a part of the electrode and diaphragm could fall dry if the liquid level in the stack drops. The effects on the performance of the electrodes and diaphragm are unknown. The diaphragm is easily wetted and will probably remain wetted due to the capillary forces. The gas crossover through the diaphragm could increase if the diaphragm would dry out. This could lead to approaching the explosion limits and therefore forms a safety risk. From the measured data two large ramps can be seen, of up to ca. 20% per min at 60°C. No problems have been listed for these events and operation was continued. It is therefore expected that the short term effect is not very important. The long term effect of dry out should be determined.

The liquid levels directly after ramp-down are not equal on both sides of the diaphragm due to different gas holdups before ramp-down. The static pressure at the bottom of the liquid column will temporarily differ on both sides of the diaphragm until the pressure is balanced by the produced gas or the pressure from the gas-liquid separators. The diaphragm could tear or gas crossover could increase due to a differential pressure difference. Both situations would pose a safety risk.

During ramp up gas is suddenly produced which will start to push liquid out of the cell. In reality friction and the inertia of the liquid in the cell will delay the outflow allowing pressure to build up in the stack. The volume of hydrogen produced is twice the volume of oxygen produced assuming equal pressure on both sides. This could lead to a pressure difference over the diaphragm. From information supplied by Nouryon it is known that the cathodic compartment is larger than the anodic compartment. The manufacturer's reason is unknown, but the fact that a larger volume of gas is produced in the cathodic compartment seems like a logical explanation.

Liquid level in separators

The collapse of the liquid column in the stack creates a void. No lye is flowing out of the stack during the time it takes to refill this void. The gas-liquid separator is drained due to constant operation of the pump. The effect on the separation of product gases and the lye is unknown. If the gas-liquid separators would be drained completely a direct connection is created through the balancing line. This leads to a safety risk as well as potential damage to the equipment.

The pump is always circulating lye to ensure flow to the stack. The gas-liquid separator is drained by this pump. The maximum freshwater flow added to the cell in the simulation is 3.6 m^3/h. The pump will then drain the gas-liquid separator at a rate of 7.9 m^3/h. The amount drained from the gas-liquid compartment becomes smaller if the freshwater flow increases. This could therefore be used to prevent very low liquid levels in the separator.

Balancing line

The dimensions and material of the balancing lines are not exactly known. It has been assumed that the balancing of the separator liquid levels happens instantly. In reality this is not the case and a pressure change in one compartment will have a delayed effect in the other. Further processing can cause the pressure at the top of the liquid surfaces to differ.

Corrosion

In order to operate more efficiently one of the options would be to allow operation temperatures higher than 80°C. Although it should be confirmed by the operator or manufacturer the limit of 80°C is likely caused by the increasing corrosivity of the lye in combination with relatively cheap electrolyzer materials. Since these materials could degrade faster at higher temperatures it could be beneficial to operate at lower efficiency and by doing so increasing the lifetime of components.

F

Step time analysis

The controllers use certain values in the model as input to control the process, the liquid level in the oxygen gas-liquid separator controlling the inflow of freshwater for example. If the timestep becomes too large, the pump will drain the separator completely while the controller will only 'notice' the liquid level has dropped below the threshold in the next timestep. By then the model cannot calculate a heat capacity and/or liquid outflow for the separator and a simulation error occurs.

The current from dataset 2 has been used to simulate electrolyzer behaviour for different timesteps. These can be found in the figures below. The timesteps that have been plotted are 1, 10, 100 and 500 seconds. For larger timesteps the model becomes unstable and result in calculation errors. As can be observed the simulation using a timestep of 1 and 10 seconds shown nearly no difference whereas the 100s timestep simulation starts to show obvious deviations. Therefore 10 seconds was used to as the simulation timestep for the validation of the model.

G

Demiwater feed flow

From the rise in liquid level between 32% and 34% the feed rate of demiwater can be determined. While the liquid level rises water is also consumed by the reaction and lost as water vapor in the product streams. Therefore in reality the feed flow is expected to be higher than the the slope of the increasing liquid level would suggest. Therefore the fresh feed inflow was determined by varying the volumetric feed in the simulation and then comparing the simulation result with the measured data. When the slopes during the liquid level rise were parallel that demiwater feed rate was used. The measured and simulated liquid levels using a demiwater feed of 3.6 m^3/h.

While the liquid level decreases noise can be seen in both the simulation and the measured data. This can be fully attributed to the noise in the input current. This current has a variation of ±20 A around the average value and causes the gas holdup in the cell to vary. Because the outflow of liquid to the gas-liquid separator is increased when the current rises and decreases when the current drops, the liquid level is subsequently varying in the same manner.

H

Heat balance at different temperatures

In this simulation the temperature is increased slowly such that all parameters can reach steady state. In Figure H.1 the influence of temperature on the size of the dissipative effects is shown. A current density of 1650 A/m^2 is constantly applied. If the cell operates at higher temperature, not only will

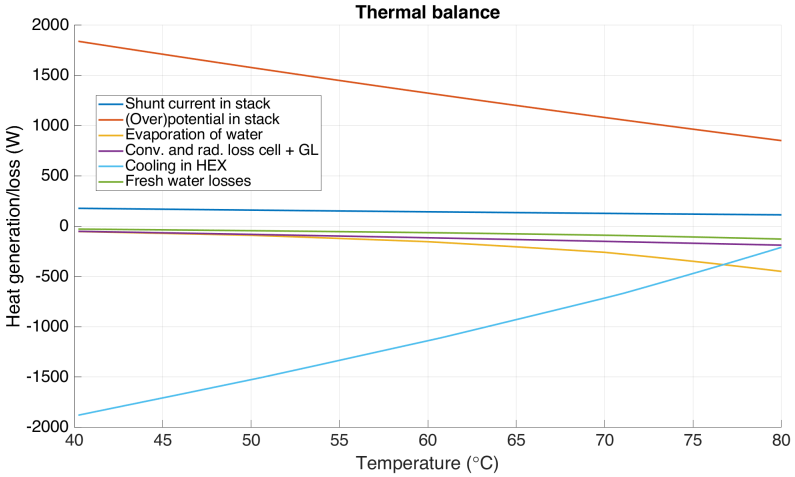

Figure H.1: The steady state heat balance of the system at 3500 A for varying temperatures

the internal resistances of the stack decrease but evaporation of water and heat losses to the exterior will also significantly increase. These effects cause the required cooling to decrease. The temperature is a self dampening mechanism that decreases the rate of temperature increase when it moves towards temperatures that could pose safety risks.

NEL Ramp claim assessment

The following plot shows the effect of a 10%/min ramp up from 750 A to 5000 A. The effect is very similar to the sudden ramp up situations. The response was very similar to the simulations in Situation 1: Ramp up from low load and Situation 2: Ramp down from full load. Only the liquid level has been shown, because the slower ramp has a small effect on the liquid levels during ramp up and down.

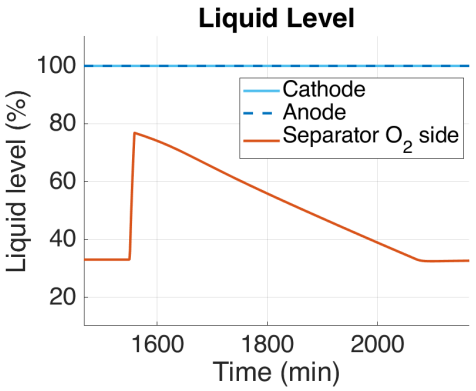

(a) Liquid level of a ramp up of 10%/min

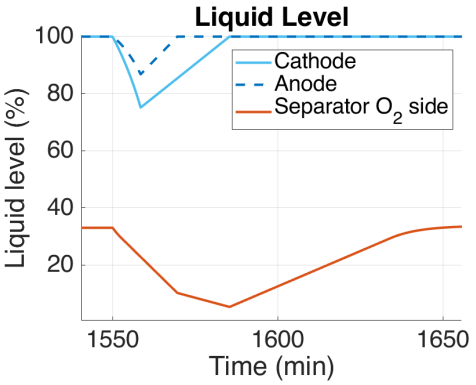

(b) Liquid level of a ramp down of 10%/min

J

Preliminary comparison: Gas holdup

By comparing the simulated and measured liquid levels, the gas holdup used in this research can be assessed. The liquid level rise during ramp up is related to a current density increase leading to an increase in gas holdup. If the current density is increased, the extra holdup forces lye out of the stack. The volume of the gas liquid separators is known and therefore an estimation of the amount of liquid pushed out of the stack can be made. The data can only be compared when the measured liquid levels are not influenced by the inflow of demiwater. This happens at the end of day 1 and during day 5. Here a pressure drop causes the liquid levels to rise which stopped the demiwater inflow until liquid levels returned to the setpoint. During the liquid level decrease the current was increased stepwise by 200 A, which is roughly 95A/m^2. The small peaks in the measured liquid level represent the gas holdup increase. The increase in liquid level in the simulation is higher than in the measured level. The simulated increase was between 1.65 and 3.5 times as large as the measured data shows. This could be attributable to differences between the stack volume of the simulated compartment and the actual system. Also the pressure was increasing, especially during day one, which causes the gas volume to decrease and therefore dampen the effects on the liquid level. More information is required to validate the gas holdup of the actual system.

K

Preliminary calculation: Backflow

From the measured liquid levels of dataset 2 two ramp down events occur. The first ramp down is not a pure ramp down and some delay is present. The second ramp down is a straight line.

From the datapoints of the second ramp down it has been determined that the liquid level drops 10.92% in 100 seconds. This means if both separators are 5.8 m^3 the volume leaving the separators is 1.26 m^3. During this time the amount that is removed due to the circulation of the pump is 0.32 m^3. The only other way to lose lye is backflow into the stack. The calculated backflow would be roughly 4 times larger than the outflow generated by the pump. The datapoints are measured only each 100 seconds and therefore causes uncertainty in the outflow to the pump. Therefore further research should validate this statement.

TU Delft

Nouryon

2020